Supplementary Information

Cycloaddition of CO_2 with Epoxide Bearing Oxindole Scaffold by MOF Based Heterogeneous Catalyst at Ambient Condition

Bhavesh Parmar,[a,b]† Parth Patel,[c,d]† Renjith S. Pillai,[e] Raj Kumar Tak,[b,c] Rukhsana I. Kureshy,[b,c,d] Noor-ul H. Khan,*[b,c,d] and Eringathodi Suresh*[a,b]

[a]Analytical and Environmental Science Division and Centralized Instrument Facility, [c]Inorganic Materials and Catalysis Division, CSIR-Central Salt and Marine Chemicals Research Institute, G. B. Marg, Bhavnagar-364 002, Gujarat, India.

[b]Academy of Scientific and Innovative Research (AcSIR), Ghaziabad 201 002, India.

[d]Charotar University of Science & Technology, Changa-388 421, Anand, Gujarat, India.

[e]Department of Chemistry, Faculty of Engineering and Technology, SRM Institute of Science and Technology, Kattankulathur 603 203, Chennai, India.

E-mail: nhkhan@csmcri.res.in; esuresh@csmcri.res.in; sureshe123@rediffmail.com

† These authors contributed equally.

X-ray Crystallography

The crystallographic data and refinement for **CoMOF-2**, epoxides and cyclic carbonates are provided in **Table S1**-**S2**. Crystal of suitable size was selected from the mother liquor and immersed in paratone oil and then mounted for data collection. Single crystal X-ray data for **CoMOF-2** was collected at 150 K using a Bruker SMART APEX CCD diffractometer with graphite-monochromatized Mo-Kα radiation (λ = 0.71069 Å). For Spiro-epoxy oxindole (five) substrates and Spiro-cyclic carbonate products (six), Single crystal X-ray data was collected at 100 K using a Bruker D8 QUEST (PHOTON)

diffractometer. The linear absorption coefficients, scattering factors for the atoms, and the anomalous dispersion corrections were obtained from International Tables for X-ray Crystallography. The data integration and reduction were processed using SAINTPLUS software.[S1] An empirical absorption correction was applied to the collected reflections with SADABS using XPREP.[S2] The structure was solved by the direct method using SHELXTL[S3] and was refined on F^2 by a full-matrix least-squares technique using the SHELXL-2014[S4] program package. Non-hydrogen atoms were refined anisotropically and the hydrogen atoms attached to the organic moiety were stereochemically fixed. The void volumes of the framework was estimated by the *PLATON* program.[S5] The disordered solvent molecules present in **CoMOF-2** could not be located from the difference Fourier map hence, *SQUEEZE* function of the *PLATON* program was used to eliminate the contribution of the electron density in the solvent region from the intensity data.[S6] The solvent accessible void volume and the corresponding electron counts/unit cell estimated was 1115.4 $Å^3$/178.1 $eÅ^{-3}$ for **CoMOF-2**. Furthermore, the accessible solvent volume is 23% of unit cell volume as calculated by PLATON. This electron count corresponds to disordered methanol and water molecules (tentatively 2 water and 1 methanol) present in the unit cell as solvent of crystallization. The contribution of the disordered guest solvent molecules were removed, and final refinement was performed. The disordered solvent molecules are not included in the molecular formula of **CoMOF-2** in the structure refinement, CIF file and crystallographic Table. CCDC numbers 1889952-1889962 corresponds to all the compounds reported in

this manuscript and this data can be obtained free of charge from The Cambridge Crystallographic Data Center via www.ccdc.cam.ac.uk/data_request/cif

Table S1. Crystal Data and Refinement Parameters for **CoMOF-2**, **S1**, **S2**, **S4, S5** and **S8**.

Identification code	**CoMOF-2**	**S1**	**S2**	**S4**	**S5**	**S8**
Chemical formula	$CoC_{20}H_{18}N_4O_7$	$C_{16}H_{13}NO_2$	$FC_{16}H_{12}NO_2$	$ClC_{16}H_{12}NO_2$	$ClC_{16}H_{12}NO_2$	$C_{12}H_{11}NO_2$
Formula weight (g/mol)	485.31	251.27	269.27	285.72	285.72	201.22
Crystal Color	Red	Colorless	Yellow	Yellow	Colorless	Colorless
Crystal Size (mm)	0.30 x 0.15 x 0.05	0.22 x 0.05 x 0.03	0.35 x 0.06 x 0.05	0.25 x 0.21 x 0.06	0.19 x 0.03 x 0.03	0.38 x 0.07 x 0.03
Temperature (K)	150(2)	110(2)	100(2)	100(2)	100(2)	100(2)
Crystal System	Monoclinic	Monoclinic	Monoclinic	Monoclinic	Orthorhombic	Monoclinic
Space Group	C 2/c	P 2_1/n	P 2_1	P 2_1/n	P 2_1 2_1 2_1	P 2_1/c
a(Å)	15.685(3)	4.4997(2)	4.4827(14)	7.8627(4)	4.4361(13)	4.7337(2)
b(Å)	17.095(4)	14.0758(4)	14.316(5)	10.8463(5)	14.128(4)	13.8010(6)
c(Å)	18.757(4)	19.4268(6)	20.111(6)	15.5275(7)	20.646(6)	15.0392(7)
α(°)	90	90	90	90	90	90
β(°)	99.516(3)	94.892(2)	90.662(9)	101.428(2)	90	91.764(2)
γ(°)	90	90	90	90	90	90
Z	8	4	4	4	4	4
V(Å^3)	4960.2(19)	1225.95(8)	1290.5(7)	1297.95(11)	1294.0(7)	982.04(8)
Density (Mg/m^3)	1.300	1.361	1.386	1.462	1.467	1.361
μ(mm^{-1})	0.735	0.090	0.102	0.294	0.295	0.093
F(000)	1992	528	560	592	592	424
Reflections Collected	13087	10506	25314	14689	12102	12093
Independent Reflections	4867	2088	4582	2222	2272	2443
R_{int}	0.0355	0.0472	0.1110	0.0274	0.1417	0.0485
Number of parameters	301	224	361	229	230	180
GOF on F^2	1.065	1.083	1.049	1.114	1.055	1.045
Final R_1/wR_2 (I ≥2σ(I))	0.0555/0.1574	0.0392/0.0822	0.0842/0.2013	0.0360/0.0826	0.0667/0.1566	0.0429/0.0962
Weighted R_1/wR_2 (all data)	0.0680/0.1638	0.0583/0.0920	0.1363/0.2293	0.0411/0.0861	0.1359/0.1991	0.0672/0.1130
CCDC number	1889952	1889953	1889954	1889955	1889956	1889957

Table S2. Crystal Data and Refinement Parameters for **P1**, **P2**, **P3**, **P4**, **P6** and **P8**.

Identification code	**P1**	**P2**	**P3**	**P4**	**P8**	**P6**[S7]
Chemical formula	$C_{17}H_{13}NO_4$	$FC_{17}H_{12}NO_4$	$C_{18}H_{15}NO_4$	$ClC_{17}H_{12}NO_4$	$C_{13}H_{11}NO_4$	$C_{11}H_9NO_4$
Formula weight (g/mol)	295.28	313.28	309.31	329.73	245.23	219.19
Crystal Color	Colorless	Colorless	Colorless	Colorless	Yellow	Colorless
Crystal Size (mm)	0.18 x 0.06 x 0.02	0.35 x 0.05 x 0.02	0.40 x 0.04 x 0.03	0.16 x 0.06 x 0.03	0.48 x 0.38 x 0.37	0.32 x 0.18 x 0.09
Temperature (K)	100(2)	100(2)	100(2)	100(2)	100(2)	100(2)
Crystal System	Monoclinic	Monoclinic	Monoclinic	Monoclinic	Triclinic	Monoclinic
Space Group	P $2_1/n$	P $2_1/n$	P $2_1/n$	P $2_1/c$	$P\bar{1}$	P $2_1/n$
a(Å)	5.1708(3)	5.03340(10)	4.9753(3)	15.7135(8)	8.8246(7)	5.39360(10)
b(Å)	17.8665(10)	17.9971(5)	18.1847(9)	5.1889(3)	8.9370(5)	18.5534(5)
c(Å)	15.1355(9)	15.4892(4)	15.9790(9)	18.3986(11)	9.1845(7)	9.8897(3)
α(°)	90	90	90	90	101.879(2)	90
β(°)	92.435(2)	91.5620(10)	91.834(2)	98.680(2)	103.683(2)	97.3110(10)
γ(°)	90	90	90	90	118.505(2)	90
Z	4	4	4	4	2	4
V(Å^3)	1397.02(14)	1402.59(6)	1444.95(14)	1482.96(14)	573.76(7)	981.61(4)
Density (Mg/m^3)	1.404	1.484	1.422	1.477	1.419	1.483
μ(mm^{-1})	0.101	0.115	0.101	0.278	0.107	0.115
F(000)	616	648	648	680	256	456
Reflections Collected	10609	18742	8806	10191	6624	9120
Independent Reflections	2868	3486	2453	3029	2738	2414
R_{int}	0.0297	0.0334	0.0502	0.0488	0.0148	0.0179
Number of parameters	251	208	268	256	207	181
GOF on F^2	1.072	1.047	1.048	1.043	1.046	1.057
Final R_1/wR_2 ($I \geq 2\sigma(I)$)	0.0376/0.0850	0.0357/0.0848	0.0404/0.0852	0.0433/0.0811	0.0355/0.0922	0.0355/0.0924
Weighted R_1/wR_2 (all data)	0.0526/0.0956	0.0406/0.0892	0.0601/0.0971	0.0697/0.0922	0.0370/0.0933	0.0382/0.0947
CCDC number	1889958	1889959	1889960	1889961	1889962	1824141

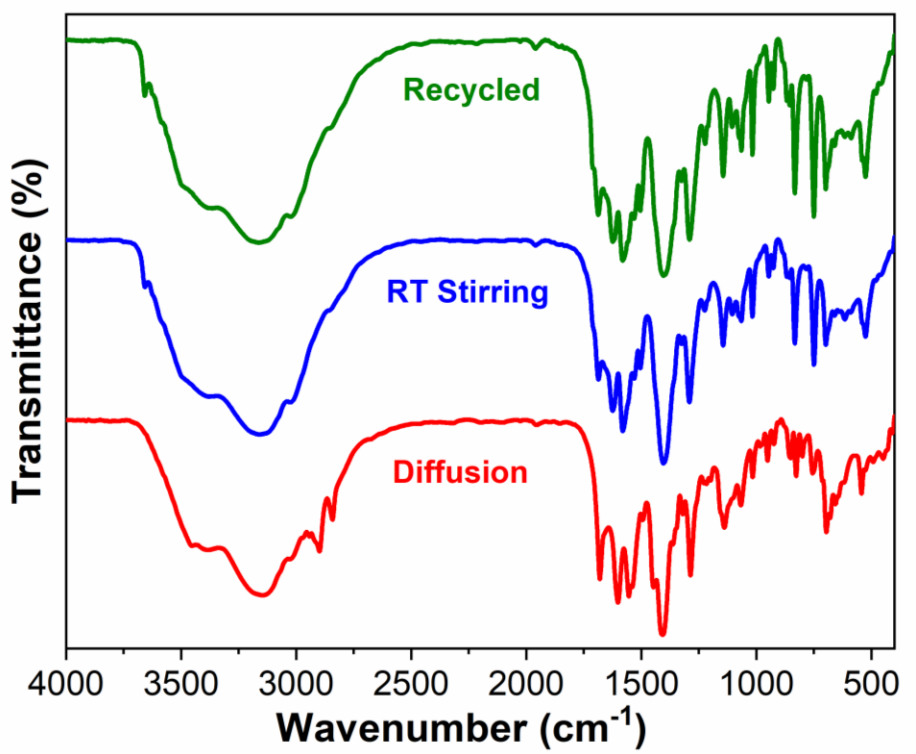

Figure S1. FTIR recorded for **CoMOF-2** (synthesized by different routes, and recovered after 6th catalytic recycle) dispersed in KBr pellets.

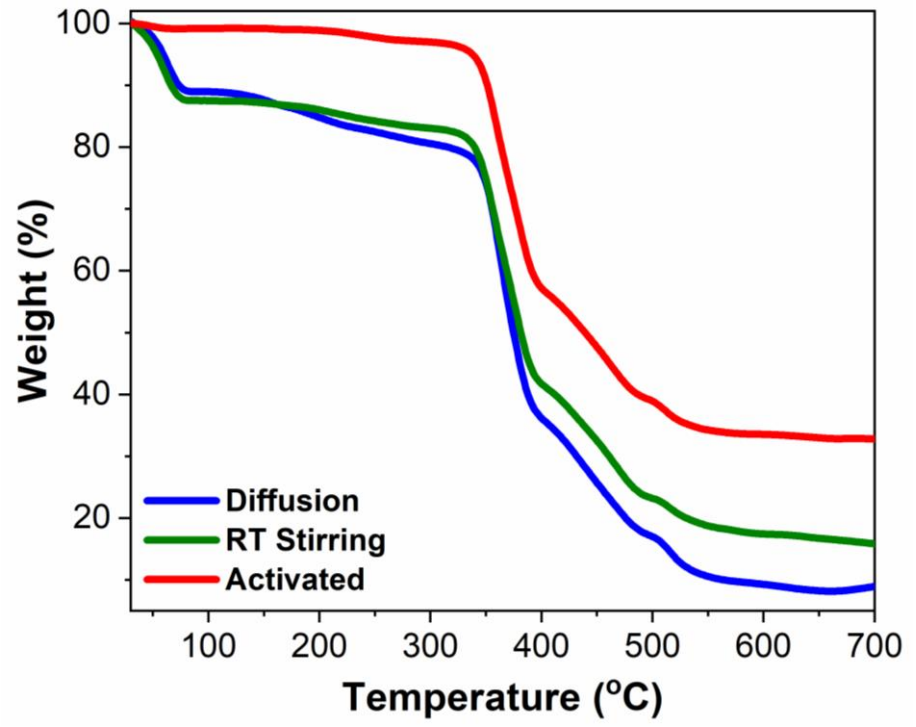

Figure S2. TGA plot for the **CoMOF-2** (synthesized by Diffusion, RT Stirring and activated MOF).

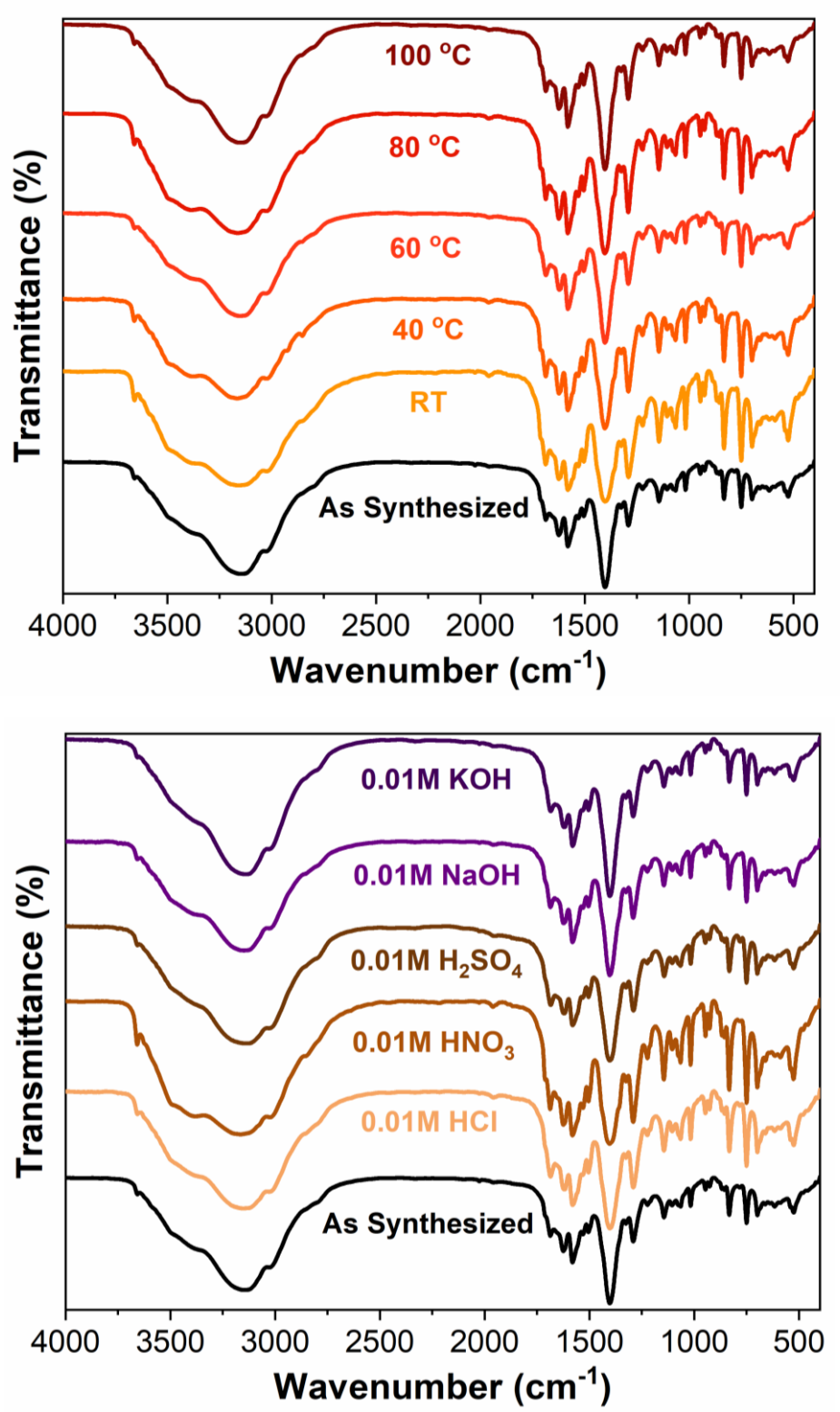

Figure S3. FTIR data of **CoMOF-2** dispersed in boiling water at different temperature (24h) and in aqueous acidic/basic solution (0.01M / 12h).

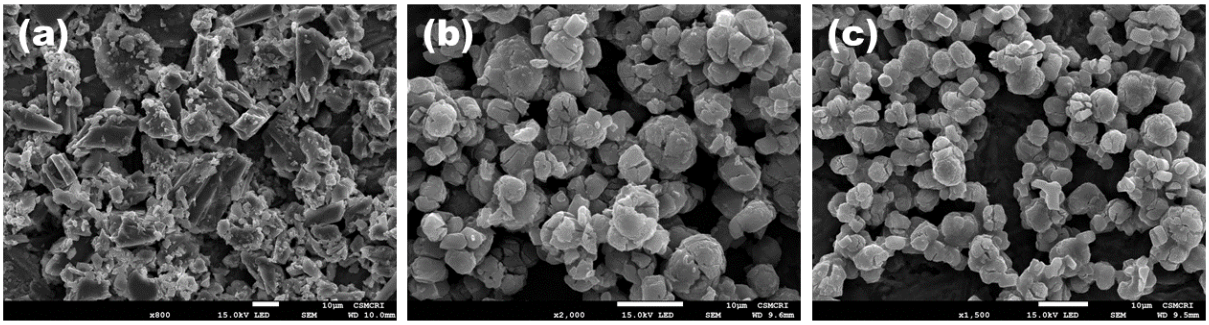

Figure S4. FE-SEM Images of **CoMOF-2** as synthesized (diffusion) (a), RT Stirring (b) and recovered after 6th catalytic recycle for epoxide conversion (c).

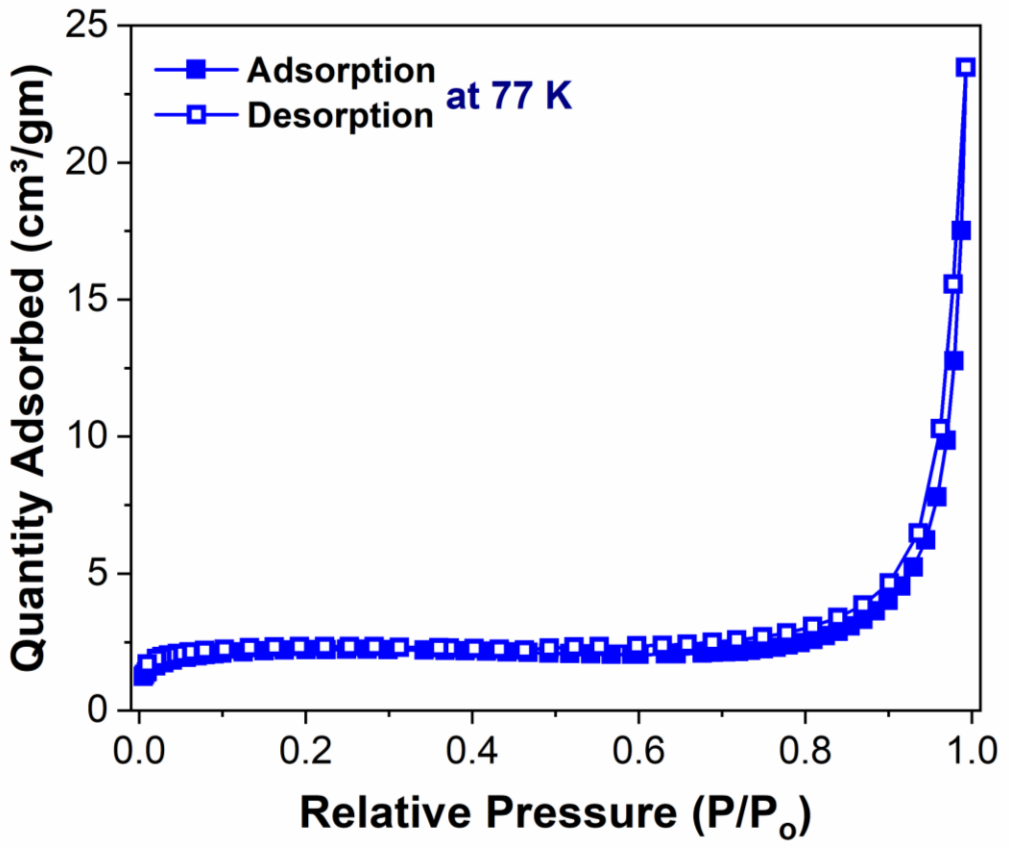

Figure S5. N_2 adsorption isotherm of **CoMOF-2'** at 77 K.

COMPUTATIONAL METHODS

Microscopic models for the host framework

The experimentally elucidated structure of **CoMOF-2** was initially geometry optimized at the Density Functional Theory (DFT) level using the CP2K package.[S8-S11] In these simulations, the positions of atoms of the framework were relaxed while the unit cell parameters were kept fixed at the values determined experimentally. All the structural optimizations were done using Perdew-Burke-Ernzerhof (PBE)[S12] functional along with a combined Gaussian basis set and pseudopotential. For Carbon, Nitrogen, Oxygen, and Hydrogen, a triple zeta (TZVP-MOLOPT) basis set was considered, while a double zeta (DZVP-MOLOPT) was applied for Cobalt.[S13] The pseudopotentials used for all of the atoms were those derived by Goedecker, Teter and Hutter.[S14] The van der Waals effects interactions were taken into account via the use of semi-empirical dispersion corrections as implemented in the DFT-D3 method.[S15]

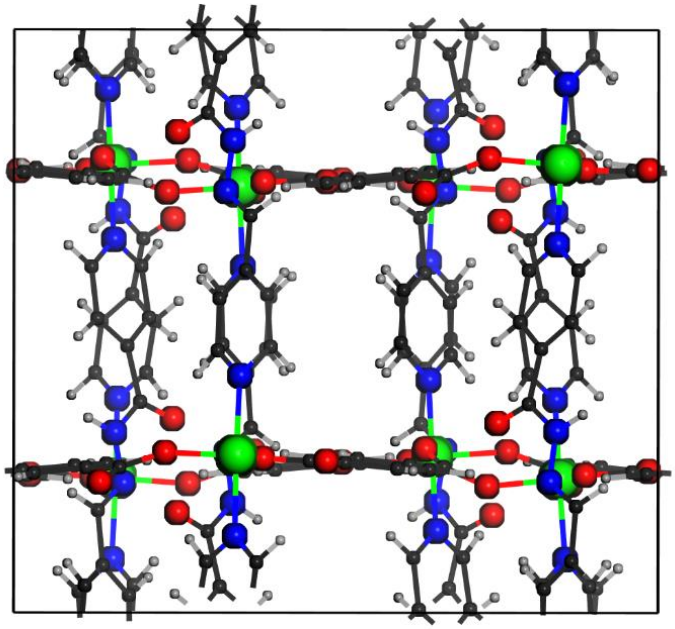

Figure S6. The single unit cell (1×1×1 simulation box) considered for the DFT calculations viewed along *c* for **CoMOF-2**. (Gray, carbon; blue, nitrogen; white, hydrogen; red, oxygen; green, cobalt).

The atomic point charges for all framework atoms of the **CoMOF-2** (**Figure S6**) were obtained using the REPEAT method proposed by Campana *et al.*,[S16] which was recently implemented into the CP2K code based on a restrained electrostatic potential framework.[S17]

Force fields

The interaction between the **CoMOF-2** framework and the CO_2 molecules was modelled using the sum of a 12-6 Lennard-Jones (LJ) contribution and a coulombic term. The Universal force field (UFF) was adopted to describe the LJ parameters for the atoms of the **CoMOF-2** framework (**Figure S6 and Table S3**).[S18] In this work, CO_2 has been modeled as a rigid molecule through the EPM2 intermolecular potential (**Table S4**).[S19]

Table S3. LJ potential parameters for the atoms of the **CoMOF-2.**

Atomic type	UFF	
	σ (Å)	ε/k_B (K)
C	3.431	52.841
H	2.571	22.143
N	3.261	34.724
O	3.118	30.195
Co	2.562	7.045

Table S4. Potential parameters and partial charges for the adsorbates.

Atomic type	σ (Å)	ε/k_B (K)	q (e)
CO_2_C	2.757	28.129	0.6512
CO_2_O	3.033	80.507	-0.3256

GCMC Simulations

Grand Canonical Monte Carlo (GCMC) simulations were carried out at two different temperatures, 273 K and 298 K, for **CoMOF-2** in order to predict the single component adsorption of CO_2. These calculations were performed using the RASPA simulation code.[S20] The simulation box was made of 6 (2×3×1) unit cells of **CoMOF-2**. Short-range dispersion forces were truncated at a cutoff radius of 12 Å while the interactions between unlike force field centers *a* and *b* were treated by means of the Lorentz-Berthelot combination rules; $\varepsilon_{ab} = \sqrt{\varepsilon_a \varepsilon_b}$, $\sigma_{ab} = (\sigma_a + \sigma_b)/2$, where ε_a and σ_a are the LJ parameters for the species *a*. The long-range electrostatic interactions were handled using the Ewald summation technique. The fugacities for each adsorbed species at a given thermodynamic condition were computed with the Peng-Robinson equation of state (EoS).[S21] For each state point, 5×10^7 Monte Carlo steps have been used for both equilibration and production runs. Three types of trials were considered for the molecules: (i) translation or rotation, (ii) creation/deletion and (iii) exchange of molecular identity. The adsorption enthalpy at low coverage (Δh) for each gas was calculated through configurational-bias Monte Carlo simulations performed in the NVT ensemble using the revised Widom's test particle insertion method.[S22] Additionally, in order to gain insight into the configurational distribution of the adsorbed species in **CoMOF-2**, some additional data were calculated at different pressure including the radial distribution functions (RDF) between the guests and the host.

Computational predictions

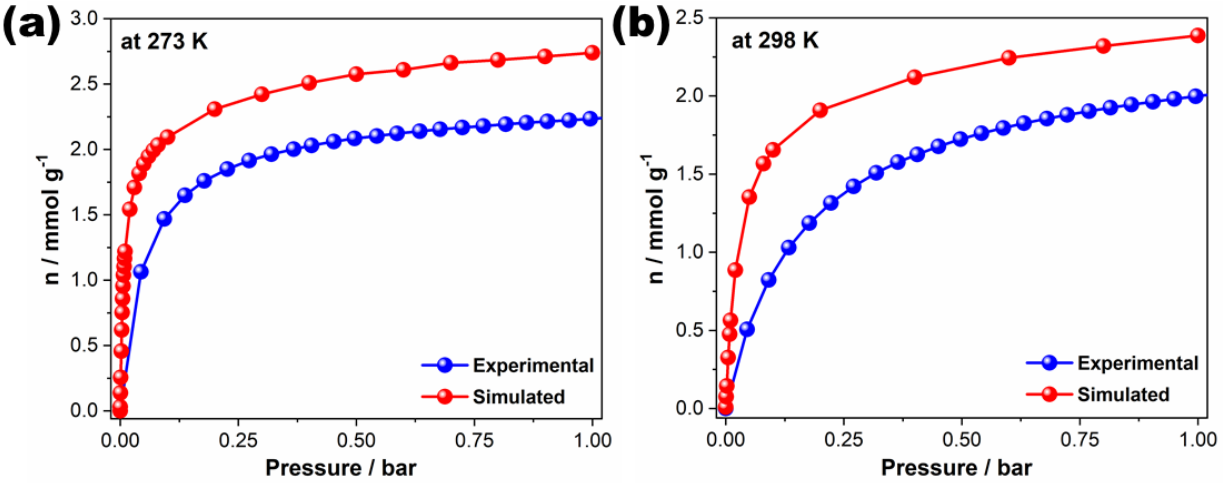

Figure S7. Comparison of the single component simulated isotherms for CO_2 (circles) with the experimental data (squares) in **CoMOF-2** at 273 K (a) and 298 K (b).

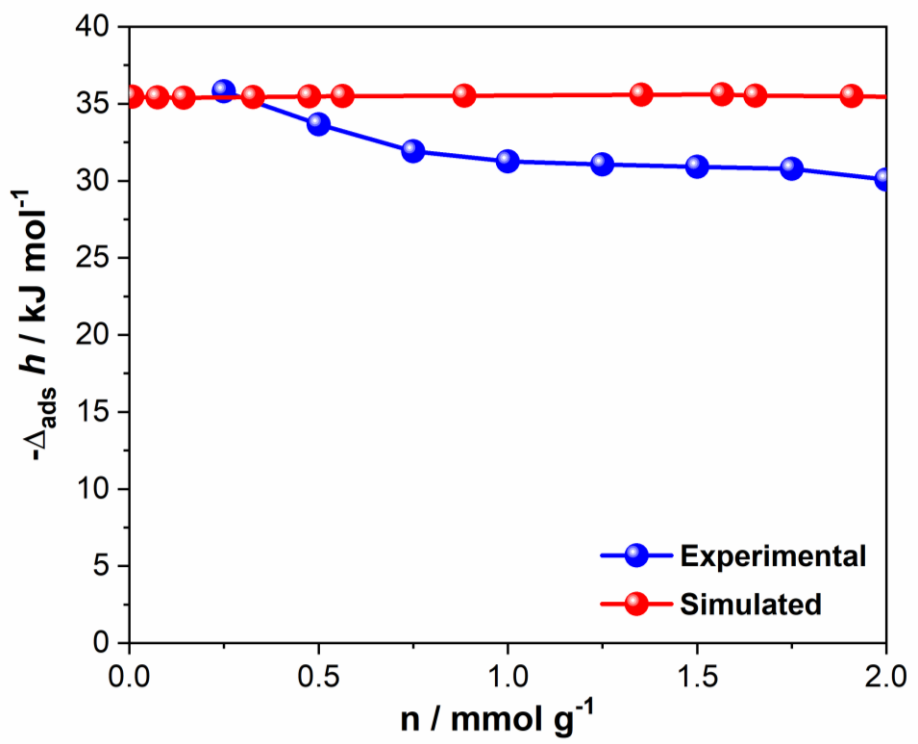

Figure S8. Comparison of the simulated adsorption enthalpy (circles) for CO_2 with the experimental data (squares) in **CoMOF-2**.

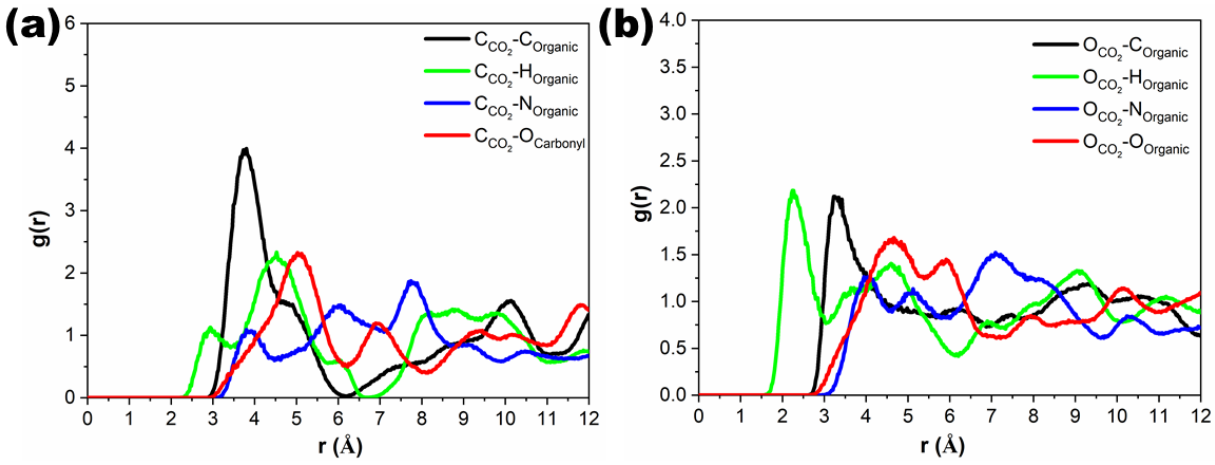

Figure S9. Radial distribution functions (RDF) between CO_2 and the atoms of the MOF framework (Organic carbon, $C_{organic}$: black, Organic hydrogen, $H_{organic}$: green, and Carbonyl group of amide functions, $O_{carbonyl}$: red) extracted from the single component adsorption in **CoMOF-2** at 1 bar and 298 K: Carbon of CO_2: C_{CO2} (a) and Oxygen of CO_2: C_{CO2} (b).

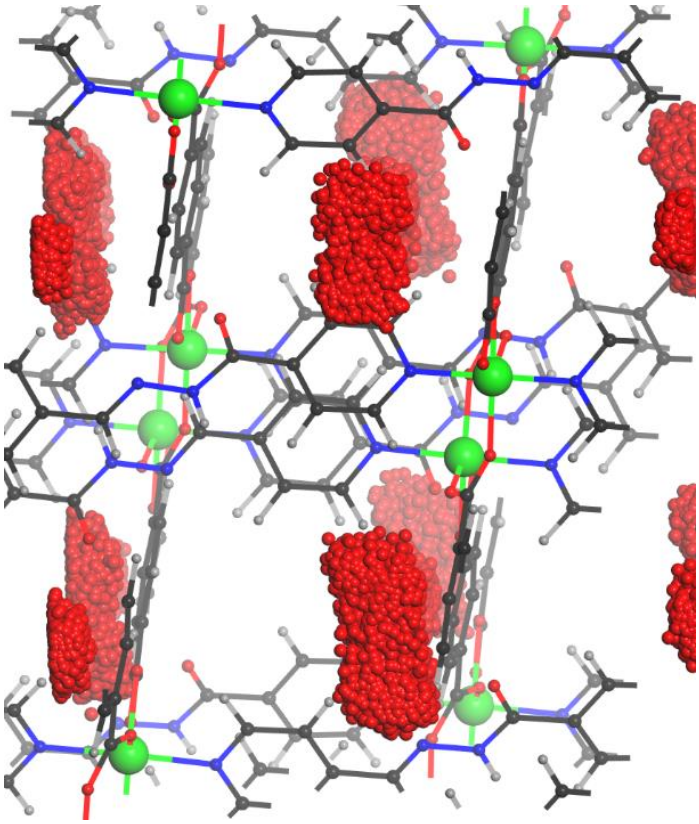

Figure S10. Maps of the occupied positions of CO_2 (red dots) in 500 equilibrated frames for a given pressure of 1 bar and at 298 K for **CoMOF-2**, color code for the atoms: C (dark grey), N (blue), O (red), Co (violet), H (light grey).

Table S5. Solvent Screening in cycloaddition of spiroepoxy oxindole with CO_2 using catalyst **CoMOF-2**.*

Entry	Solvent	**S1** Conversion (%)	**P1** Selectivity (%)
1	Acetone	92	12
2	**Acetonitrile**	**99**	**99**
3	Dichloromethane	91	98
4	Methanol	92	12
5	Toluene	76	86

*Reaction conditions: Epoxide = 0.15 mmol, Catalyst mol%: **CoMOF-2** = 5.0 mol%; Potassium iodide (KI) = 0.2 mol%; P_{CO2} = 1 atm, 8 h, and 40 °C, 600 rpm.

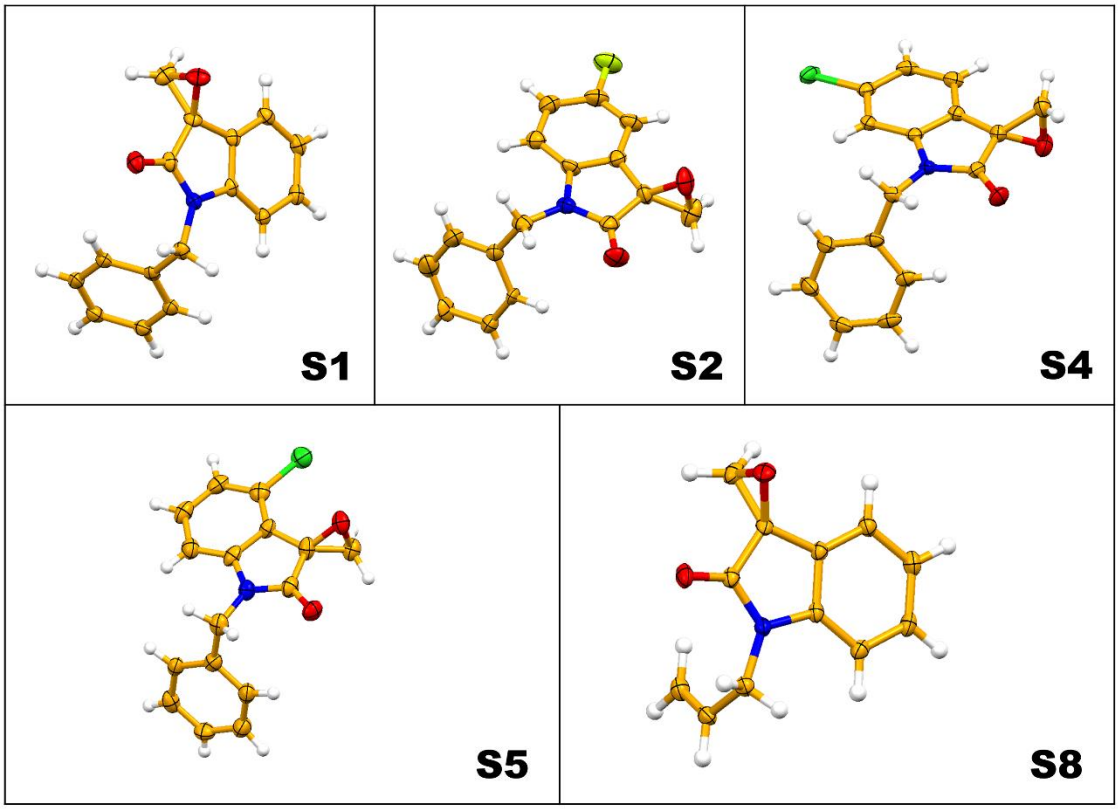

Figure S11. Thermal Ellipsoids Plot depicting the crystal structure of Spiro-Epoxy Oxindoles (**S1**, **S2**, **S4**, **S5** and **S8**; 50% probability factor for the thermal ellipsoids).

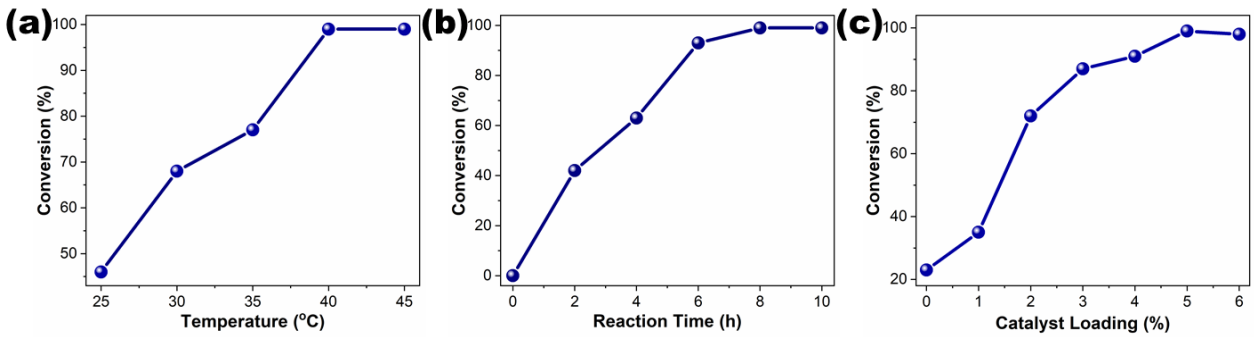

Figure S12. Effect of temperature (°C) (a), reaction time (b), and catalyst loading (c) on 1-benzylspiro[indoline-3,4'-[1,3]dioxolane]-2,2'-dione (**P1**) formation. (Reaction conditions: **1S** = 0.15 mmol, 600 rpm. Catalyst mol%: **CoMOF-2** = 5.0 mol%; TBAB/TBAI/KI = 0.2 mol%; Solvent = CH_3CN; P_{CO2} = 1 atm. Selectivity 99%)

Computational Methods for catalytic mechanism

Optimization and frequency calculations of all the clusters are done at the M06/BS1 level[S23] of density functional theory (DFT) using Gaussian 16 program.[S24] In BS1, cobalt center is defined with LANL2DZ basis set and pseudopotentials for core electrons while 6–31G(d,p) basis set is used to define all other atoms. All the transition states are characterized by a single imaginary frequency along the reaction coordinate, whereas all the intermediates are confirmed to be a minimum by locating zero imaginary frequency in the vibrational analysis. DFT calculations were done with intermediates and transitions states illustrating the cycloaddition reaction of Spiro-Epoxy oxindole and CO_2 to form product using the **CoMOF-2**/KI catalyst is shown in the **Figure S13**. Here, we considered the **CoMOF-2** catalyst as a cluster model and its atomic positions kept frozen for all the DFT calculations. To that purpose, a cluster model was first appropriately cut from the periodic structure to fairly describe the **CoMOF-2** framework with the following chemical composition: $[Co_2(\mathbf{BDC})_4(\mathbf{L})_4]$. The bulky KI is represented simply by the Iodide ion (I^-) which is directly involved in the rate determining step. For the calculation, the

total relative energy of the cluster model of **CoMOF-2** (catalyst), nucleophile (I^-), CO_2, and Spiro-Epoxy oxindole (isolated reactants) was consider to zero energy and the optimized structures of reactant complexes are depicted in **Figure S13** & **Scheme S1**. In the case of each stages of catalytic reaction (e g. IC, Int, TS, FC etc.), the relative energies were computed with respect to the sum of the total energies of the corresponding gas phase molecules as represented in Equation 1.

$$E_{relative} = E_{stage} - \left(E_{Co-MOF-2+I} - E_{CO_2} - E_{epoxide}\right) \qquad (1)$$

Where $E_{stage}, E_{Co-MOF-2+I}$, E_{CO_2} and $E_{epoxide}$ represents the total energies of the **CoMOF-2** + I^- with adsorbates at each reaction stage, the empty **CoMOF-2** + I^- catalyst, gas phase CO_2 and gas phase Spiro-Epoxy oxindole, respectively. The relative energy profile is further rescaled to keep in the order of previously reported similar catalytic reaction involving MOF. Equation 1 defines negative values as exothermic and positive values as endothermic processes. It is observed that an initial structure followed by an intermediate (Int-1) is formed by the interaction of the oxygen atom of the Spiro-Epoxy oxindole with the Cobalt metal center, which is considered as the initial step for the catalytic path way and its energy is very similar to the total relative energy of the cluster model of **CoMOF-2** (catalyst), nucleophile (I^-), CO_2, and Spiro-Epoxy oxindole (isolated reactants). Initially, the I^- ion was at a far distance of >5.5 Å from the alpha carbon ($\alpha C_{(epoxide)}$) of Spiro-Epoxy oxindole. Upon the introduction of I^- ion in the vicinity of the Spiro-Epoxy oxindole (Int-1) results the slightly decrease in relative energy to -2.09 kcal/mol (see **Scheme S1**). Here, the distance between O atom of Spiro-Epoxy oxindole and the

Cobalt metal atom is 4.06 Å and the I^- ion and the alpha carbon ($\alpha C_{(epoxide)}$) of the Spiro-Epoxy oxindole is 4.0 Å.

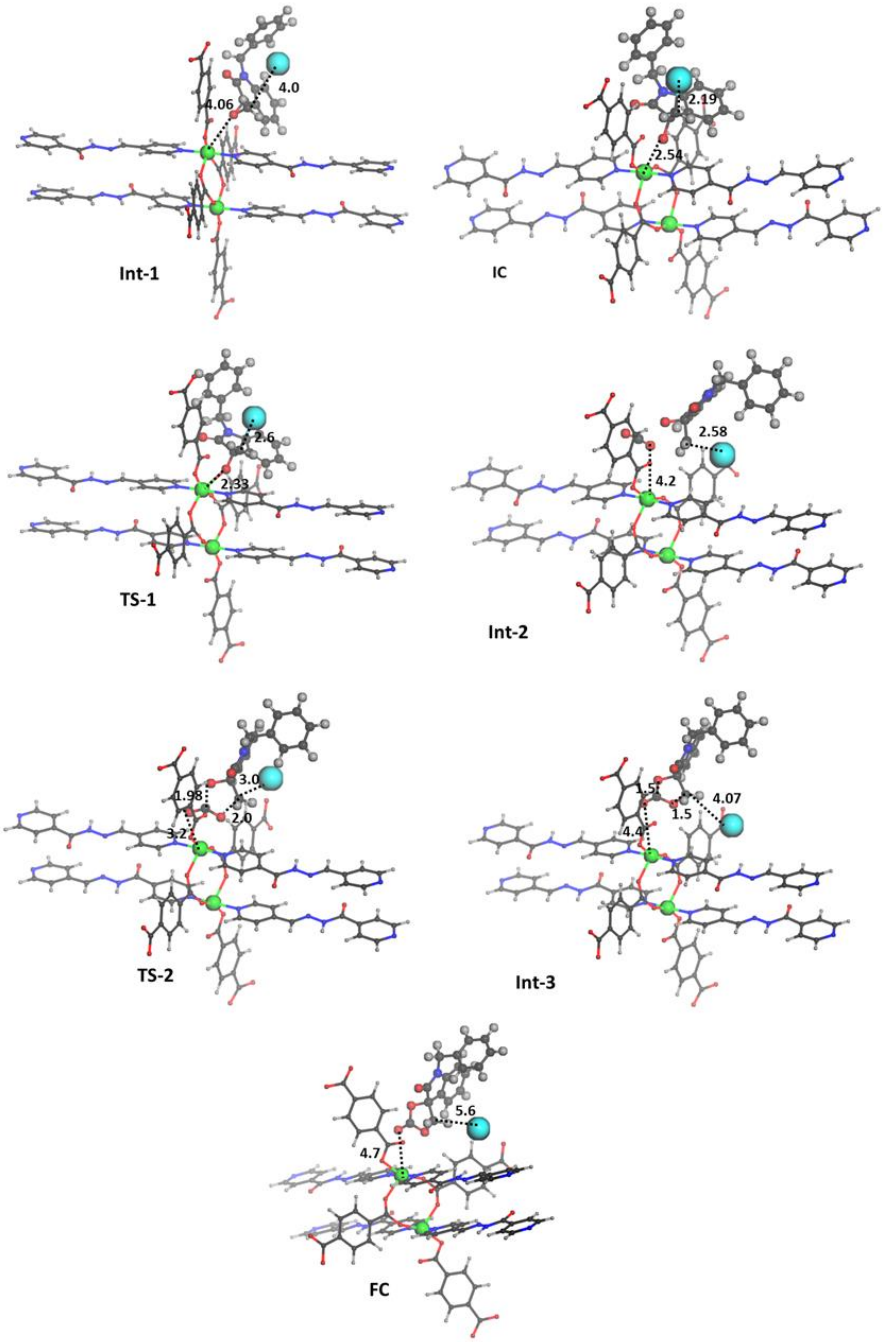

Figure S13. Local views of the mechanistic pathways of the intermediates and transitions states in the cycloaddition of Spiro-Epoxy oxindole and CO_2 using cluster model structure of **CoMOF-2** catalyst with I^- ion. color code for the atoms: C (dark grey), N (blue), O (red), Co (green), H (light grey), I(Cyan).

In the ring opening step, iodide ion makes a nucleophilic attack towards the α-carbon ($\alpha C_{(epoxide)}$) atom of Spiro-Epoxy oxindole to form an alkoxide species (IC), further this IC leads to first transition state with a relative energy of 67.9 kcal/mol. The ring opening of ($\alpha C_{(epoxide)}$) pave way for stronger Co-$O_{(C6)}$ interaction with an inter atomic distance of 2.34 Å and the newly formed $\alpha C_{(epoxide)}$-I bond with a distance of 2.57 Å. As depicted in the **Scheme S1**, the energy barrier of TS-1 for the ring opening of Spiro-Epoxy oxindole is 67.9 kcal/mol and a relative energy between the TS-1 and IC is of 17.0 kcal/mol. According to previous DFT energy profile, the higher energy barrier ring opening step is the rate determining step in the CO_2 fixation with Spiro-Epoxy oxindole. In the subsequent step, the iodide ion substituted alkoxide species (TS-1) falls into an intermediate state (Int-2) with a total energy value of 30.72 kcal/mol. It can be seen in Int-2 that a molecule of CO_2 approaches the Spiro-Epoxy oxindole with the distance of 2.58 Å. In the latter step, the CO_2 attacks the negatively charged oxygen atom of Spiro-Epoxy oxindole leading to the formation of second transition state (TS-2). In TS-2, the physical binding of CO_2 takes place between the Co and alkoxide group with a total energy value of 84.5 kcal/mol. The TS-2 involves the formation of new bonds, Co-$O_{(CO2)}$ and $O_{(CO2)}$-$\alpha C_{(epoxide)}$ with corresponding bond distances are 3.05 Å and 2.08 Å, respectively. After TS-2, the ring closure step was determined via the formation of new intermediate Int-3 with an energy of 26.05 kcal/mol. In Int-3, the positively charged carbon atom of CO_2 attacks the oxygen atom of Spiro-Epoxy oxindole leading to the formation of Spirocyclic oxindole carbonate through new $O_{(epoxide)}$-$C_{(CO2)}$ bond. Interestingly, the bond distance of $O_{(CO2)}$- $\alpha C_{(epoxide)}$ is shortened to 1.42 Å from 1.98 Å while the Co-$O_{(CO2)}$ and C-I bond distance is elongated to 4.41 Å from 3.04 Å and 4.07 Å from

3.14 Å, respectively. Finally, the detachment of Spirocyclic oxindole carbonate is located with an energy of -3.1 kcal/mol followed by the regeneration of **CoMOF-2** and I^- ion (FC).

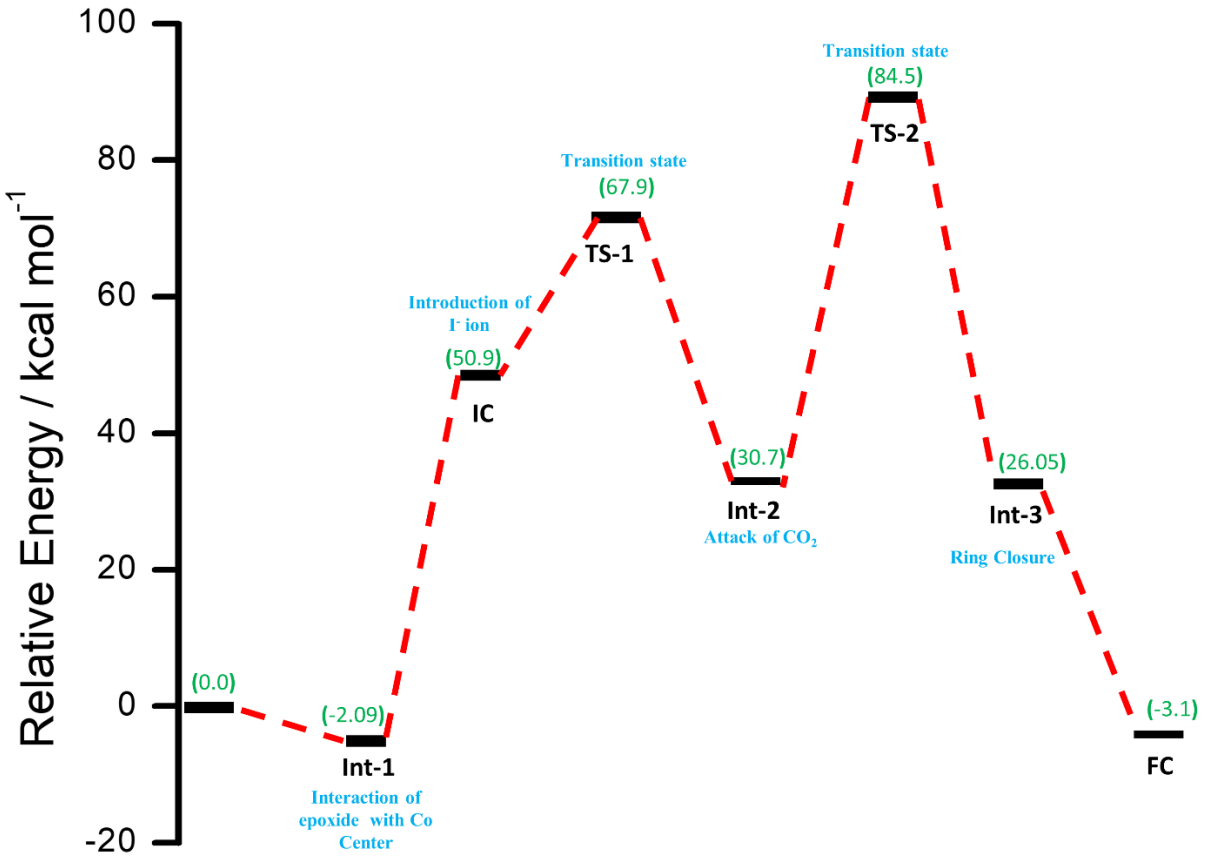

Scheme S1. Energy profile diagram of the intermediates and transitions states calculated using DFT calculation in the cycloaddition of Spiro-Epoxy oxindole and CO_2 to form Spirocyclic oxindole carbonate, using the **CoMOF-2** catalyst.

^{1}H & ^{13}C NMR analysis of Spiro-epoxy oxindole substrates and Spiro cyclic carbonate products

^{1}H and ^{13}C NMR spectra of Spiro-epoxy oxindole substrates and Spiro cyclic carbonate products involve in this study are matched well with reported in the literature.[S7,S25-S26] ^{1}H and ^{13}C NMR data are as follows.

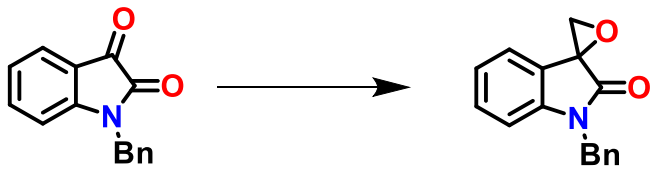

1-benzylspiro[indoline-3,2'-oxiran]-2-one (S1): ^{1}H NMR (600 MHz, $CDCl_3$) δ 7.33 (d, *J* = 4.5 Hz, 4H), 7.30 – 7.25 (m, 2H), 7.12 (d, *J* = 7.6 Hz, 1H), 7.05 (t, *J* = 7.5 Hz, 1H), 6.81 (d, *J* = 8.0 Hz, 1H), 5.04 – 4.91 (m, 2H), 3.66 (d, *J* = 6.8 Hz, 1H), 3.48 (d, *J* = 6.8 Hz, 1H). ^{13}C NMR (151 MHz, $CDCl_3$) δ 172.06, 144.41, 135.45, 130.47, 129.01, 127.99, 127.57, 123.07, 122.84, 122.34, 110.05, 56.53, 54.47, 44.46.

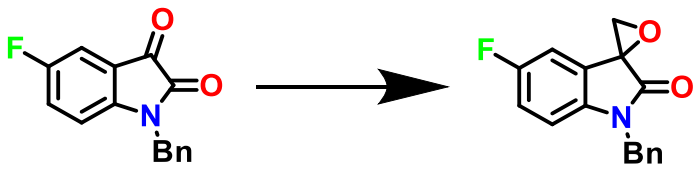

1-benzyl-5-fluorospiro[indoline-3,2'-oxiran]-2-one (S2): ^{1}H NMR (600 MHz, $CDCl_3$) δ 7.32 (tt, *J* = 15.3, 7.2 Hz, 5H), 6.99 – 6.93 (m, 1H), 6.89 – 6.84 (m, 1H), 6.72 (dd, *J* = 8.6, 4.0 Hz, 1H), 4.96 (q, *J* = 16.0 Hz, 2H), 3.67 (d, *J* = 6.0 Hz, 1H), 3.46 (d, *J* = 6.7 Hz, 1H). ^{13}C NMR (151 MHz, $CDCl_3$) δ 171.79, 158.66, 140.22, 135.14, 129.10, 128.13, 127.53, 116.91, 116.75, 110.78, 110.59, 110.42, 56.54, 54.64, 44.61.

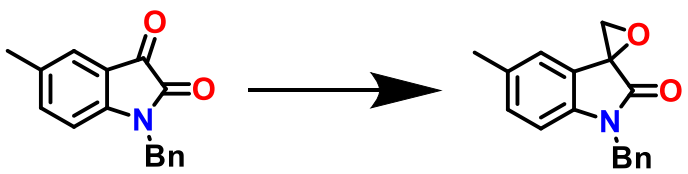

1-benzyl-5-methylspiro[indoline-3,2'-oxiran]-2-one (S3): ^{1}H NMR (600 MHz, $CDCl_3$) δ 7.36 – 7.23 (m, 5H), 7.05 (d, *J* = 7.9 Hz, 1H), 6.93 (s, 1H), 6.69 (d, *J* = 8.0 Hz, 1H), 4.95 (q, *J* = 15.6 Hz, 2H), 3.64 (d, *J* = 6.8 Hz, 1H), 3.45 (d, *J* = 6.7 Hz, 1H), 2.29 (s, 3H). ^{13}C NMR (151 MHz, $CDCl_3$) δ 172.03, 142.01, 135.56, 132.80, 130.73, 128.97, 127.92, 127.54, 123.05, 122.82, 109.83, 56.59, 54.41, 44.46, 21.07.

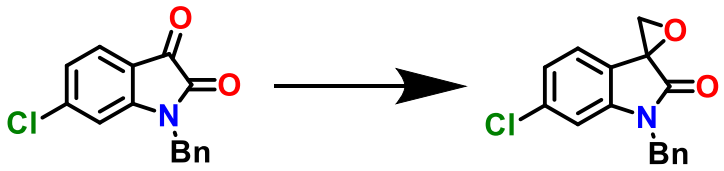

1-benzyl-6-chlorospiro[indoline-3,2'-oxiran]-2-one (S4): ^{1}H NMR (600 MHz, $CDCl_3$) δ 7.39 – 7.34 (m, 2H), 7.32 (d, *J* = 6.8 Hz, 3H), 7.03 (s, 2H), 6.81 (s, 1H), 5.00 – 4.87 (m, 2H), 3.66 (d, *J* = 6.2 Hz, 1H), 3.47 (d, *J* = 6.9 Hz, 1H). ^{13}C NMR (151 MHz, $CDCl_3$) δ 171.99, 145.53, 136.36, 134.91, 129.17, 128.23, 127.53, 123.30, 123.09, 121.22, 56.19, 54.51, 44.59.

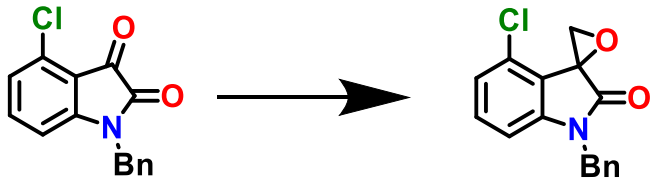

1-benzyl-4-chlorospiro[indoline-3,2'-oxiran]-2-one (S5): ^{1}H NMR (600 MHz, $CDCl_3$) δ 7.33 (d, *J* = 7.4 Hz, 2H), 7.31 – 7.26 (m, 3H), 7.18 (t, *J* = 8.2 Hz, 1H), 6.97 (d, *J* = 8.2 Hz, 1H), 6.71 (d, *J* = 7.9 Hz, 1H), 5.01 – 4.90 (m, 2H), 4.13 (d, *J* = 7.0 Hz, 1H), 3.57 (d, *J* = 7.9 Hz, 1H). ^{13}C NMR (151 MHz, $CDCl_3$) δ 171.50, 146.16, 135.02, 131.32, 130.88, 129.09, 128.14, 127.48, 124.35, 119.05, 108.53, 56.93, 50.83, 44.59.

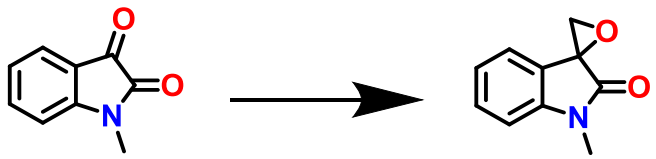

1-methylspiro[indoline-3,2'-oxiran]-2-one (S6): ^{1}H NMR (600 MHz, $CDCl_3$) δ 7.39 (q, *J* = 7.5, 6.7 Hz, 1H), 7.10 (dt, *J* = 14.9, 7.1 Hz, 2H), 6.92 (d, *J* = 7.3 Hz, 1H), 3.58 (d, *J* = 6.9 Hz, 1H), 3.44 (d, *J* = 6.9 Hz, 1H), 3.28 (s, 3H). ^{13}C NMR (151 MHz, $CDCl_3$) δ 171.90, 145.20, 130.55, 123.02, 122.80, 122.22, 108.98, 56.51, 54.21, 26.77.

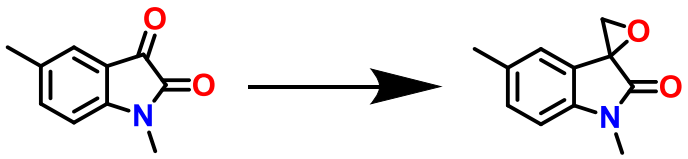

1,5-dimethylspiro[indoline-3,2'-oxiran]-2-one (S7): ^{1}H NMR (600 MHz, $CDCl_3$) δ 7.28 – 7.14 (m, 1H), 6.93 (s, 1H), 6.81 (d, *J* = 7.8 Hz, 1H), 3.57 (d, *J* = 6.6 Hz, 1H), 3.41 (d, *J* = 6.7 Hz, 1H), 3.26 (s, 3H), 2.33 (s, 3H). ^{13}C NMR (151 MHz, $CDCl_3$) δ 171.87, 142.87, 132.74, 130.78, 122.98, 122.80, 108.74, 56.59, 54.16, 26.81, 21.10.

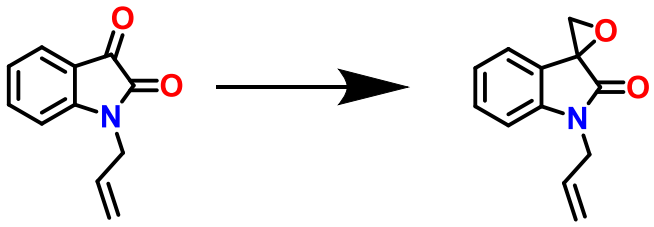

1-allylspiro[indoline-3,2'-oxiran]-2-one (S8): ^{1}H NMR (600 MHz, $CDCl_3$) δ 7.35 (t, *J* = 7.5 Hz, 1H), 7.12 (d, *J* = 7.1 Hz, 1H), 7.08 (t, *J* = 7.5 Hz, 1H), 6.93 (d, *J* = 8.0 Hz, 1H), 5.86 (ddt, *J* = 16.1, 10.4, 5.2 Hz, 1H), 5.34 – 5.22 (m, 2H), 4.48 – 4.33 (m, 2H), 3.61 (d, *J* = 6.0 Hz, 1H), 3.46 (d, *J* = 6.9 Hz, 1H). ^{13}C NMR (151 MHz, $CDCl_3$) δ 171.63, 144.45, 131.17, 130.45, 122.99, 122.78, 122.29, 118.24, 109.92, 56.45, 54.36, 42.98.

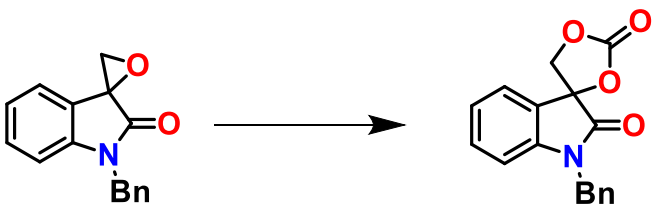

1-benzylspiro[indoline-3,4'-[1,3]dioxolane]-2,2'-dione (P1): ^{1}H NMR (600 MHz, $CDCl_3$) δ 7.46 (d, *J* = 7.6 Hz, 1H), 7.32 (dt, *J* = 28.0, 7.8 Hz, 6H), 7.15 (t, *J* = 7.5 Hz, 1H), 6.80 (d, *J* = 7.5 Hz, 1H), 4.95 (d, *J* = 15.3 Hz, 1H), 4.84 (d, *J* = 15.8 Hz, 1H), 4.78 (d, *J* = 8.6 Hz, 1H), 4.58 (d, *J* = 8.9 Hz, 1H). ^{13}C NMR (151 MHz, $CDCl_3$) δ 171.65, 153.78, 143.67, 134.53, 132.52, 129.20, 128.32, 127.49, 125.11, 124.28, 123.50, 110.55, 79.27, 70.93, 44.43.

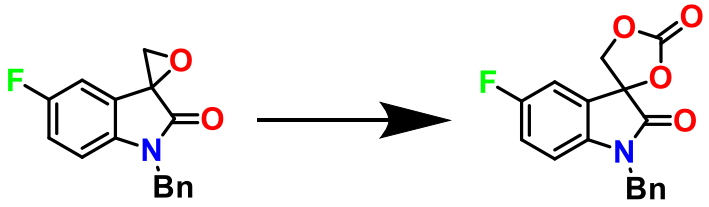

1-benzyl-5-fluorospiro[indoline-3,4'-[1,3]dioxolane]-2,2'-dione (P2): ^{1}H NMR (600 MHz, $CDCl_3$) δ 7.37 – 7.31 (m, 3H), 7.29 – 7.26 (m, 2H), 7.22 (d, *J* = 7.0 Hz, 1H), 7.05 (t, *J* = 8.7 Hz, 1H), 6.73 (dd, *J* = 8.9, 3.6 Hz, 1H), 4.95 (d, *J* = 15.6 Hz, 1H), 4.86 – 4.78 (m, 2H), 4.57 (d, *J* = 8.0 Hz, 1H). ^{13}C NMR (151 MHz, $CDCl_3$) δ 134.18, 129.29, 128.47, 127.46, 119.11, 118.95, 113.33, 113.17, 111.57, 111.52, 77.37, 77.16, 76.95, 70.82, 44.62.

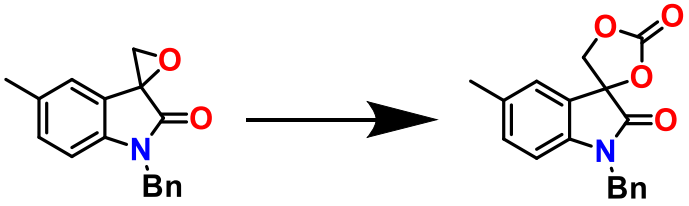

1-benzyl-5-methylspiro[indoline-3,4'-[1,3]dioxolane]-2,2'-dione (P3): ^{1}H NMR (600 MHz, $CDCl_3$) δ 7.33 (q, *J* = 9.4, 8.2 Hz, 2H), 7.30 – 7.26 (m, 4H), 7.09 (dd, *J* = 48.1, 8.2 Hz, 1H), 6.64 (dd, *J* = 32.2, 8.0 Hz, 1H), 4.93 (d, *J* = 15.1 Hz, 1H), 4.85 – 4.74 (m, 2H), 4.57 (d, *J* = 9.2 Hz, 1H), 2.32 (s, 3H). ^{13}C NMR (151 MHz, $CDCl_3$) δ 132.74, 129.16, 128.96, 128.25, 127.47, 127.33, 125.75, 110.32, 77.37, 77.16, 76.95, 70.98, 44.43, 21.07.

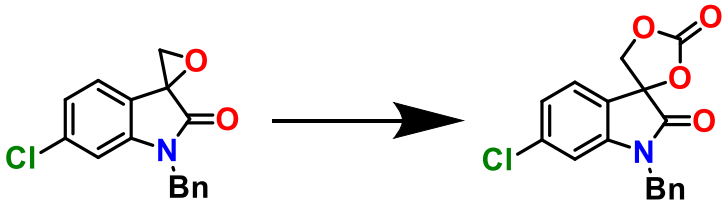

1-benzyl-6-chlorospiro[indoline-3,4'-[1,3]dioxolane]-2,2'-dione (P4): ^{1}H NMR (600 MHz, $CDCl_3$) δ 7.38 (dd, *J* = 13.8, 7.9 Hz, 3H), 7.33 (d, *J* = 6.9 Hz, 1H), 7.28 (d, *J* = 7.1 Hz, 2H), 7.13 (dd, *J* = 8.0, 2.0 Hz, 1H), 6.79 (d, *J* = 2.0 Hz, 1H), 4.93 (d, *J* = 15.5 Hz, 1H), 4.84 – 4.76 (m, 2H), 4.56 (d, *J* = 9.2 Hz, 1H). ^{13}C NMR (151 MHz, $CDCl_3$) δ 153.48, 144.91, 138.65, 133.99, 129.36, 128.57, 127.46, 126.11, 124.30, 121.79, 111.28, 78.73, 77.37, 77.16, 76.95, 70.73, 44.60.

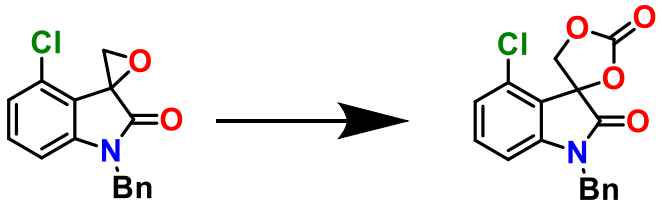

1-benzyl-4-chlorospiro[indoline-3,4'-[1,3]dioxolane]-2,2'-dione (P5): ^{1}H NMR (600 MHz, $CDCl_3$) δ 7.37 – 7.33 (m, 2H), 7.32 – 7.27 (m, 4H), 7.08 (d, *J* = 8.8 Hz, 1H), 6.71 (d, *J* = 8.2 Hz, 1H), 4.96 (d, *J* = 15.6 Hz, 1H), 4.86 – 4.81 (m, 2H), 4.75 (d, *J* = 8.6 Hz, 1H). ^{13}C NMR (151 MHz, $CDCl_3$) δ 171.14, 145.22, 134.11, 133.53, 132.83, 129.27, 128.47, 127.43, 124.78, 108.98, 79.02, 77.37, 77.16, 76.95, 68.57, 44.71.

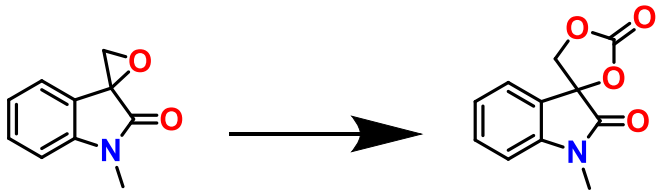

1-methylspiro[indoline-3,4'-[1,3]dioxolane]-2,2'-dione (P6): ^{1}H NMR (600 MHz, $CDCl_3$) δ 7.47 (dd, *J* = 9.9, 7.6 Hz, 2H), 7.19 (t, *J* = 7.5 Hz, 1H), 6.91 (d, *J* = 7.2 Hz, 1H), 4.72 (d, *J* = 9.1 Hz, 1H),

4.55 (d, *J* = 8.5 Hz, 1H), 3.23 (s, 3H). ^{13}C NMR (151 MHz, $CDCl_3$) δ 171.40, 153.81, 144.48, 132.62, 124.98, 124.25, 123.56, 109.52, 79.24, 70.90, 26.80.

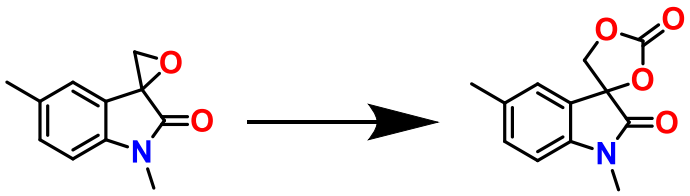

1,5-dimethylspiro[indoline-3,4'-[1,3]dioxolane]-2,2'-dione (P7): ^{1}H NMR (600 MHz, $CDCl_3$) δ 7.30 – 7.24 (m, 2H), 6.79 (d, *J* = 8.0 Hz, 1H), 4.71 (d, *J* = 9.1 Hz, 1H), 4.53 (d, *J* = 9.0 Hz, 1H), 3.21 (s, 3H), 2.37 (s, 3H). ^{13}C NMR (151 MHz, $CDCl_3$) δ 171.32, 153.87, 142.00, 134.17, 132.79, 125.65, 123.57, 109.28, 79.43, 77.37, 77.16, 76.95, 70.95, 26.81, 21.10.

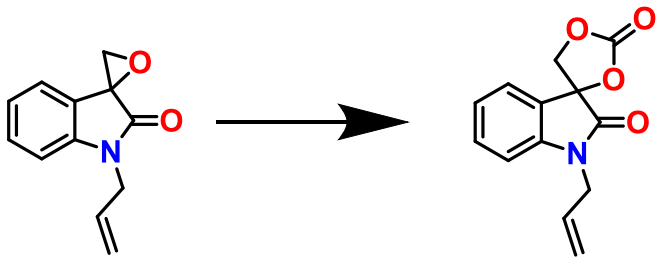

1-allylspiro[indoline-3,4'-[1,3]dioxolane]-2,2'-dione (P8): ^{1}H NMR (600 MHz, $CDCl_3$) δ 7.52 – 7.41 (m, 2H), 7.19 (t, *J* = 7.7 Hz, 1H), 6.91 (d, *J* = 7.8 Hz, 1H), 5.83 (ddt, *J* = 16.1, 10.4, 5.3 Hz, 1H), 5.33 – 5.24 (m, 2H), 4.74 (d, *J* = 9.3 Hz, 1H), 4.56 (d, *J* = 9.1 Hz, 1H), 4.34 (qd, *J* = 16.3, 5.6 Hz, 2H). ^{13}C NMR (151 MHz, $CDCl_3$) δ 171.18, 153.77, 143.76, 132.52, 130.32, 125.08, 124.22, 123.53, 118.87, 110.43, 79.18, 70.91, 42.98.

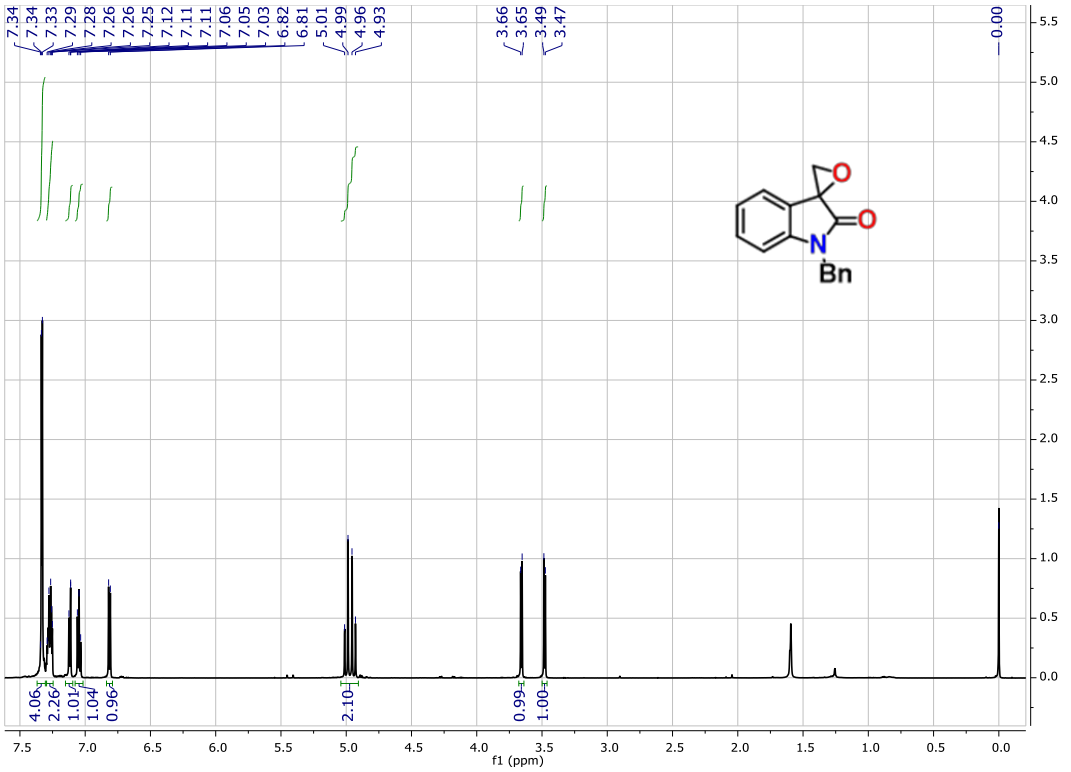

Figure S14. ^{1}H-NMR of the isolated 1-benzylspiro[indoline-3,2'-oxiran]-2-one (S1).

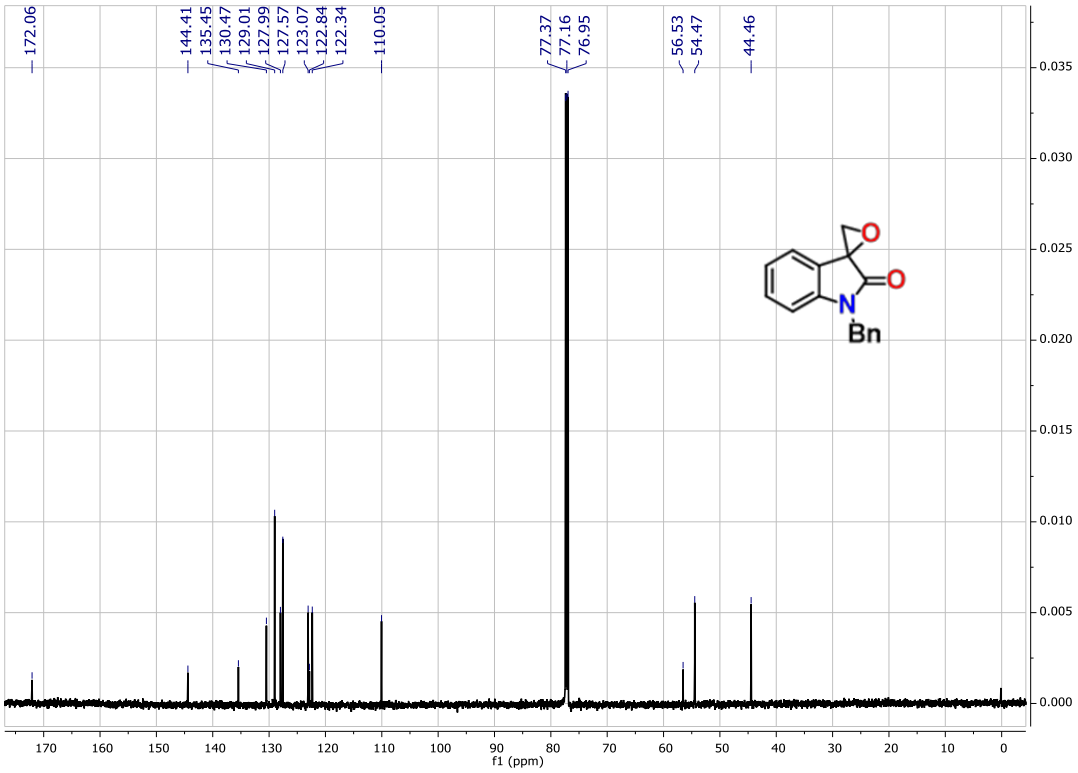

Figure S15. ^{13}C-NMR of the isolated 1-benzylspiro[indoline-3,2'-oxiran]-2-one (S1).

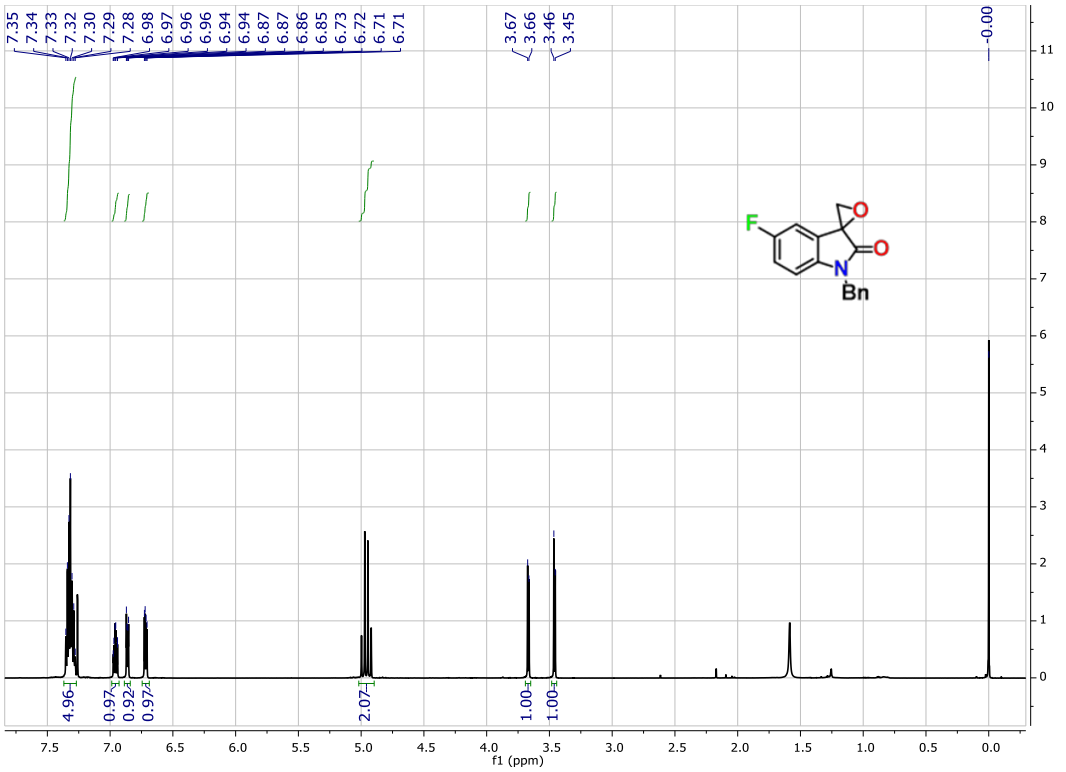

Figure S16. ^{1}H-NMR of the isolated 1-benzyl-5-fluorospiro[indoline-3,2'-oxiran]-2-one (S2).

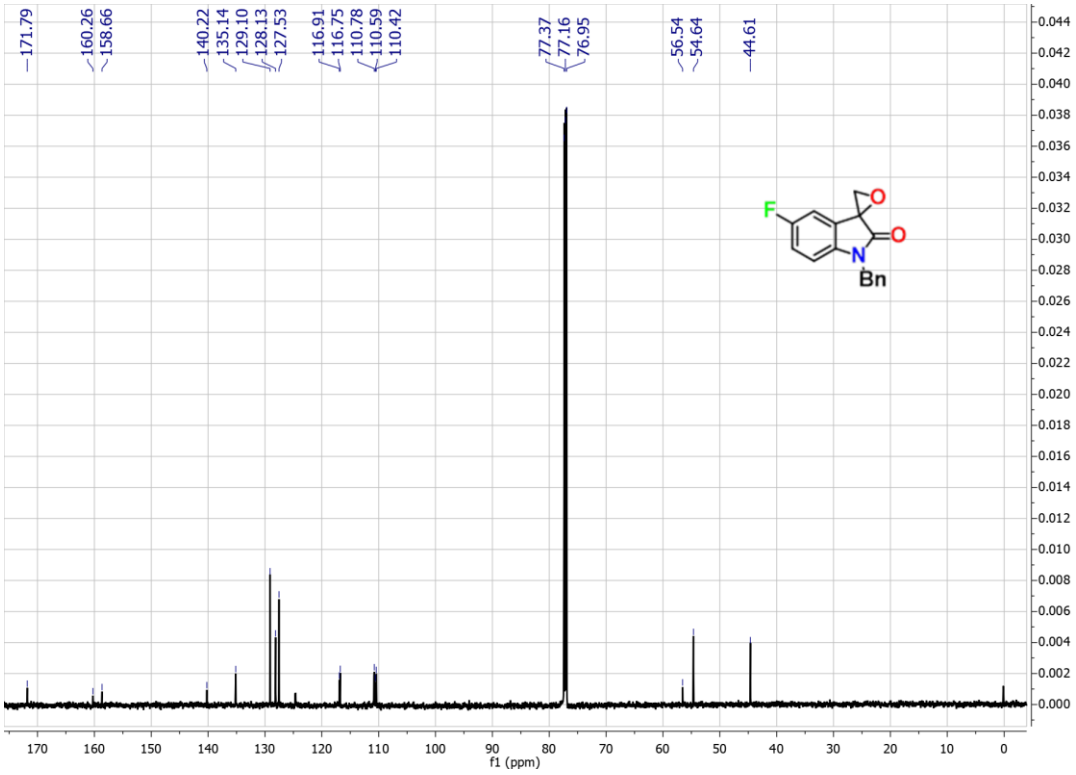

Figure S17. ^{13}C-NMR of the isolated 1-benzyl-5-fluorospiro[indoline-3,2'-oxiran]-2-one (S2).

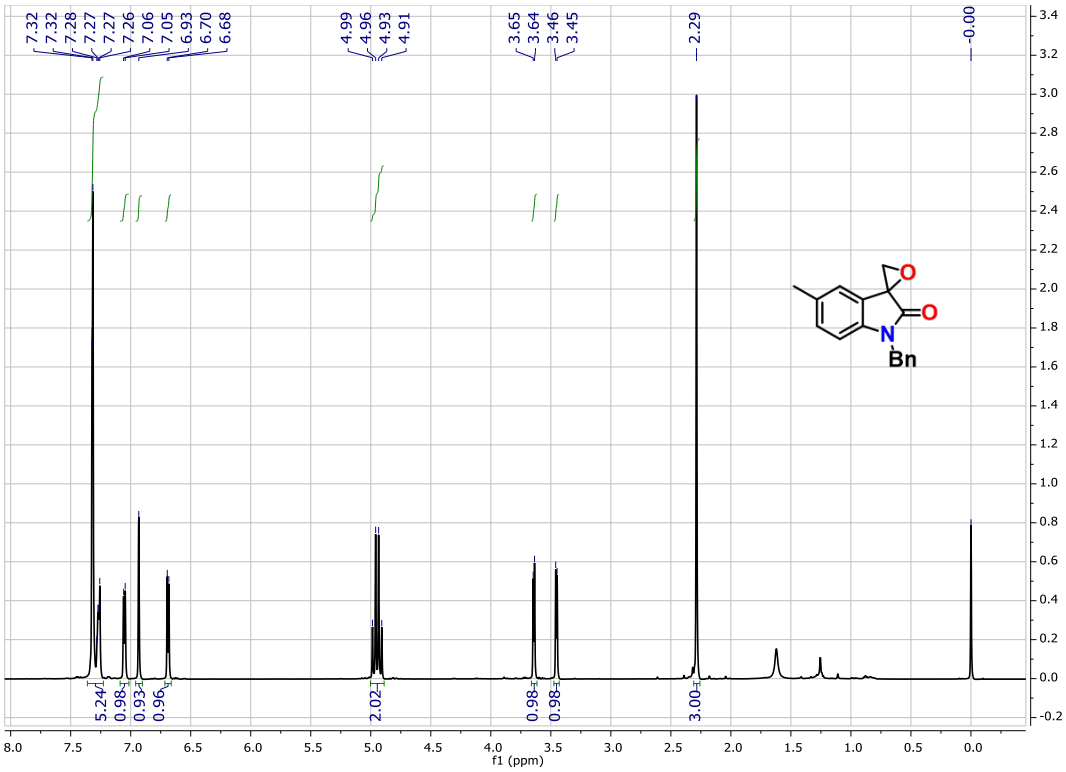

Figure S18. ^{1}H-NMR of the isolated 1-benzyl-5-methylspiro[indoline-3,2'-oxiran]-2-one (S3).

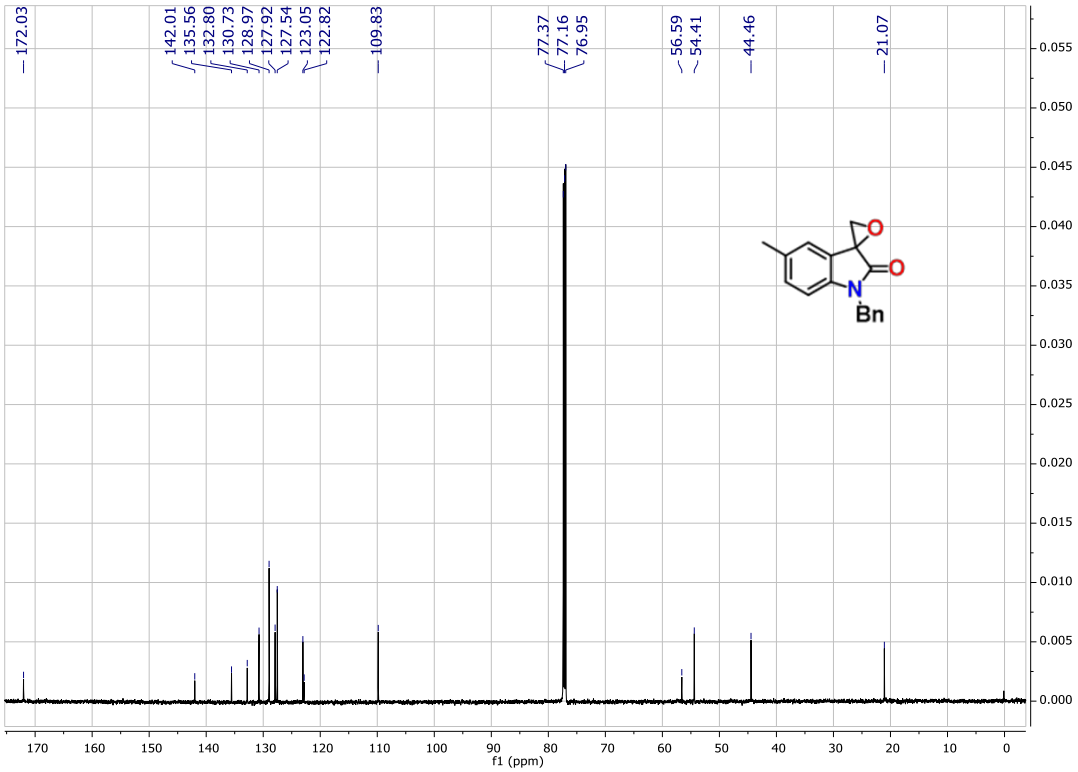

Figure S19. ^{13}C-NMR of the isolated 1-benzyl-5-methylspiro[indoline-3,2'-oxiran]-2-one (S3).

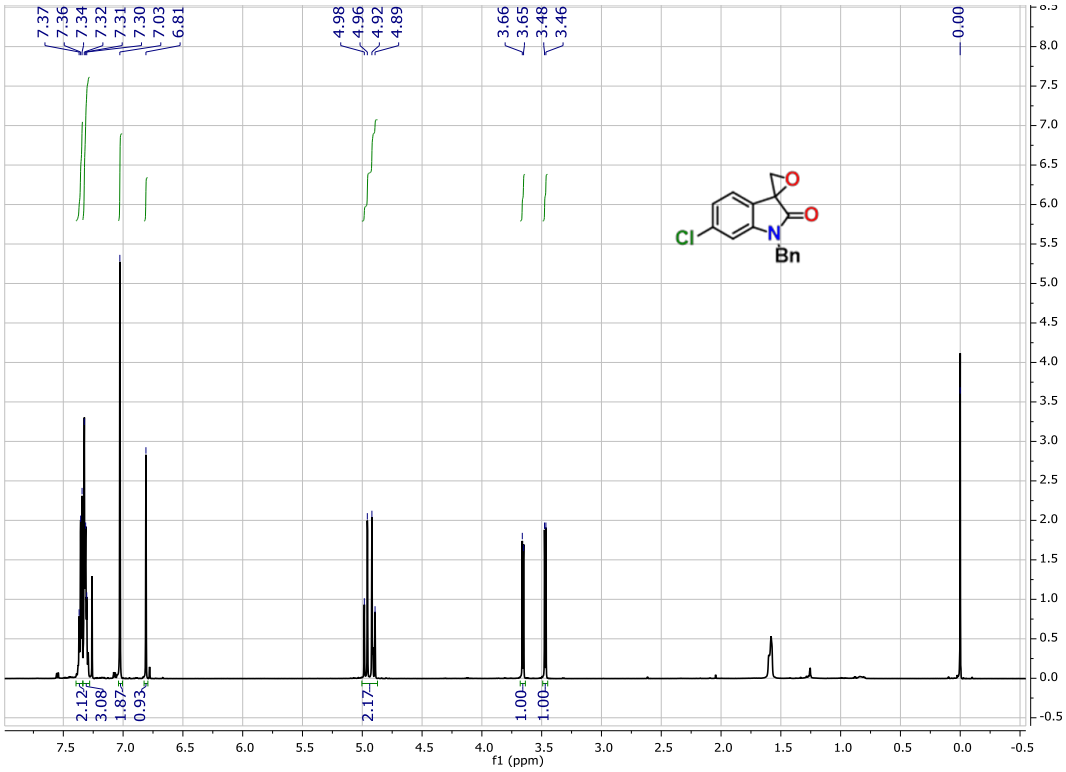

Figure S20. ^{1}H-NMR of the isolated 1-benzyl-6-chlorospiro[indoline-3,2'-oxiran]-2-one (S4).

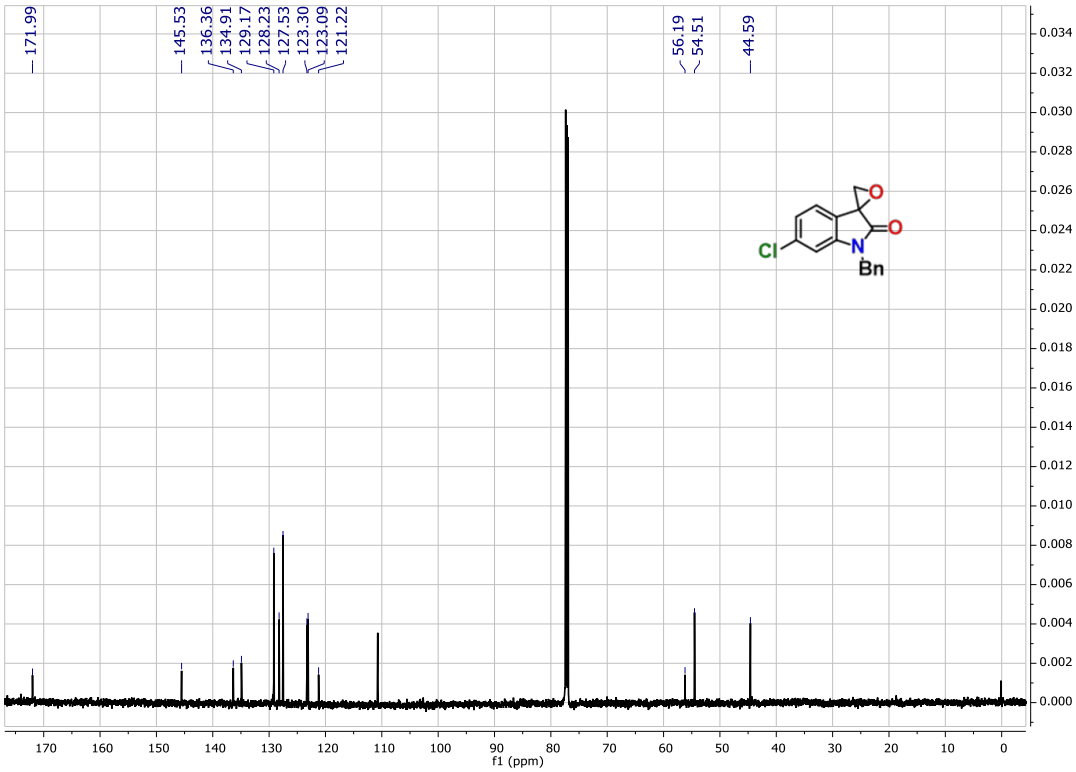

Figure S21. ^{13}C-NMR of the isolated 1-benzyl-6-chlorospiro[indoline-3,2'-oxiran]-2-one (S4).

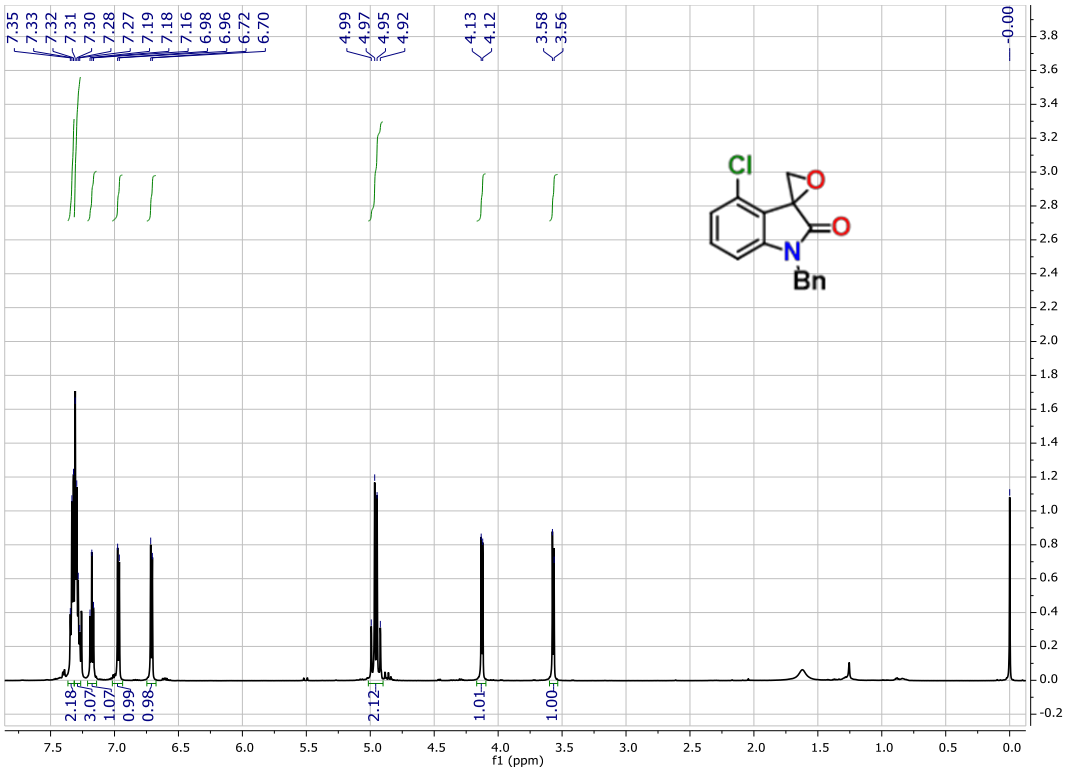

Figure S22. ^{1}H-NMR of the isolated 1-benzyl-4-chlorospiro[indoline-3,2'-oxiran]-2-one (S5).

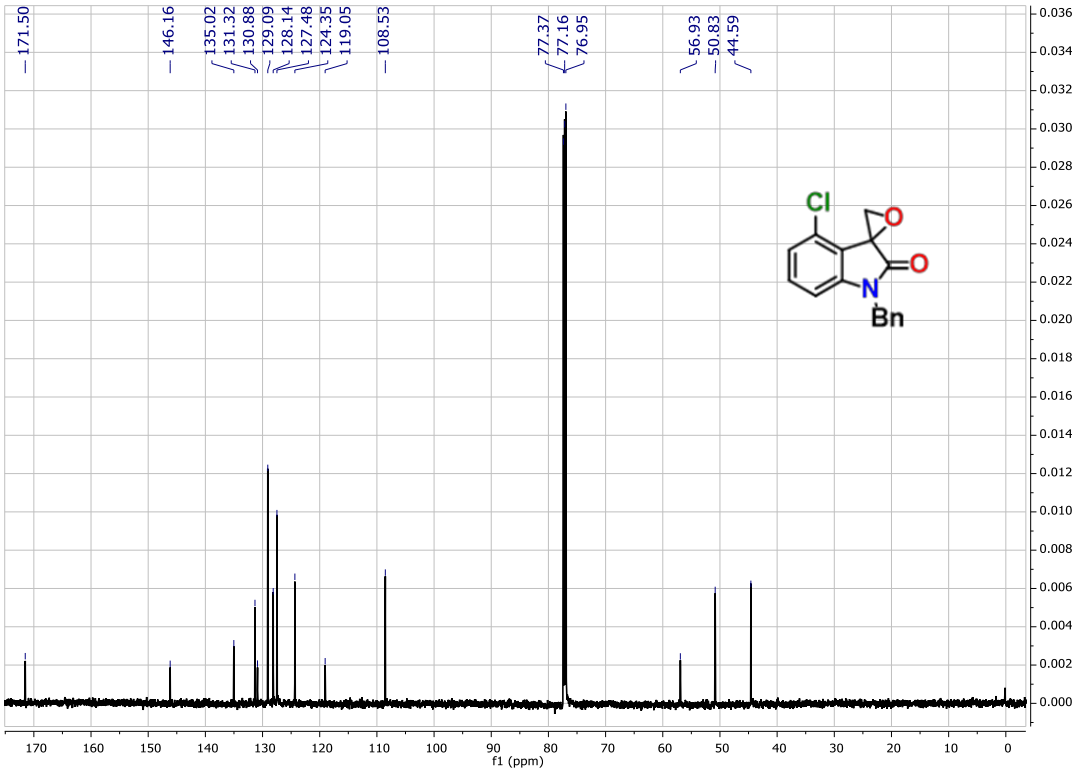

Figure S23. ^{13}C-NMR of the isolated 1-benzyl-4-chlorospiro[indoline-3,2'-oxiran]-2-one (S5).

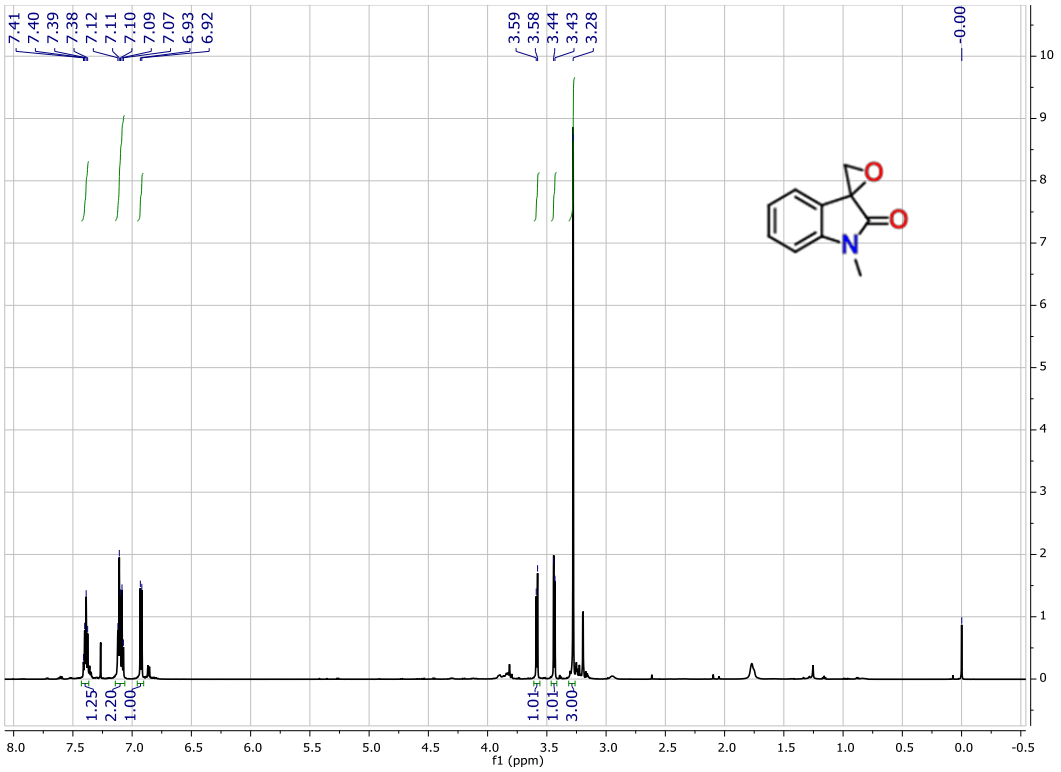

Figure S24. ^{1}H-NMR of the isolated 1-methylspiro[indoline-3,2'-oxiran]-2-one (S6).

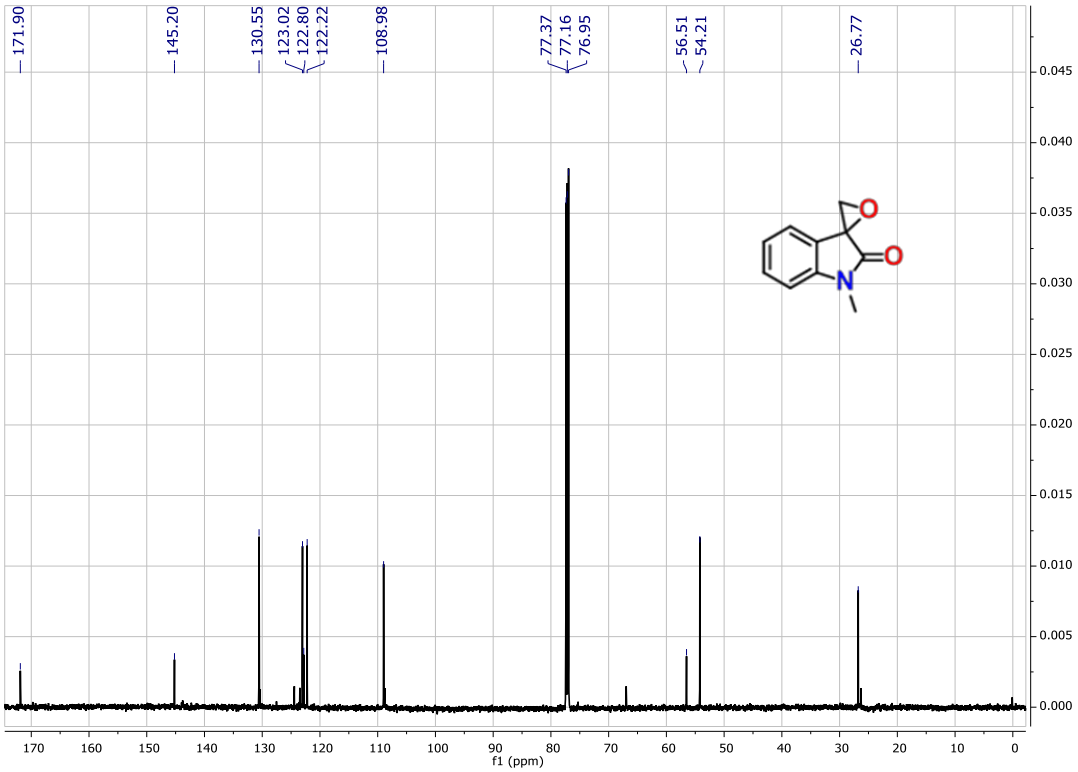

Figure S25. ^{13}C-NMR of the isolated 1-methylspiro[indoline-3,2'-oxiran]-2-one (S6).

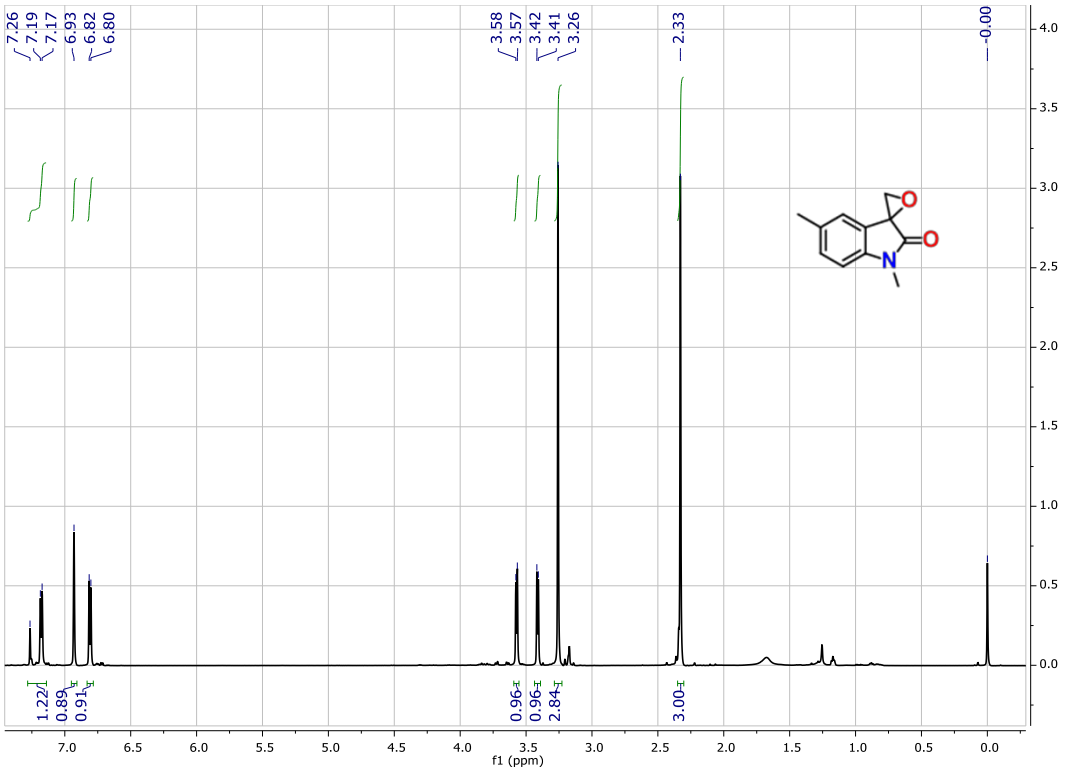

Figure S26. ^{1}H-NMR of the isolated 1,5-dimethylspiro[indoline-3,2'-oxiran]-2-one (S7).

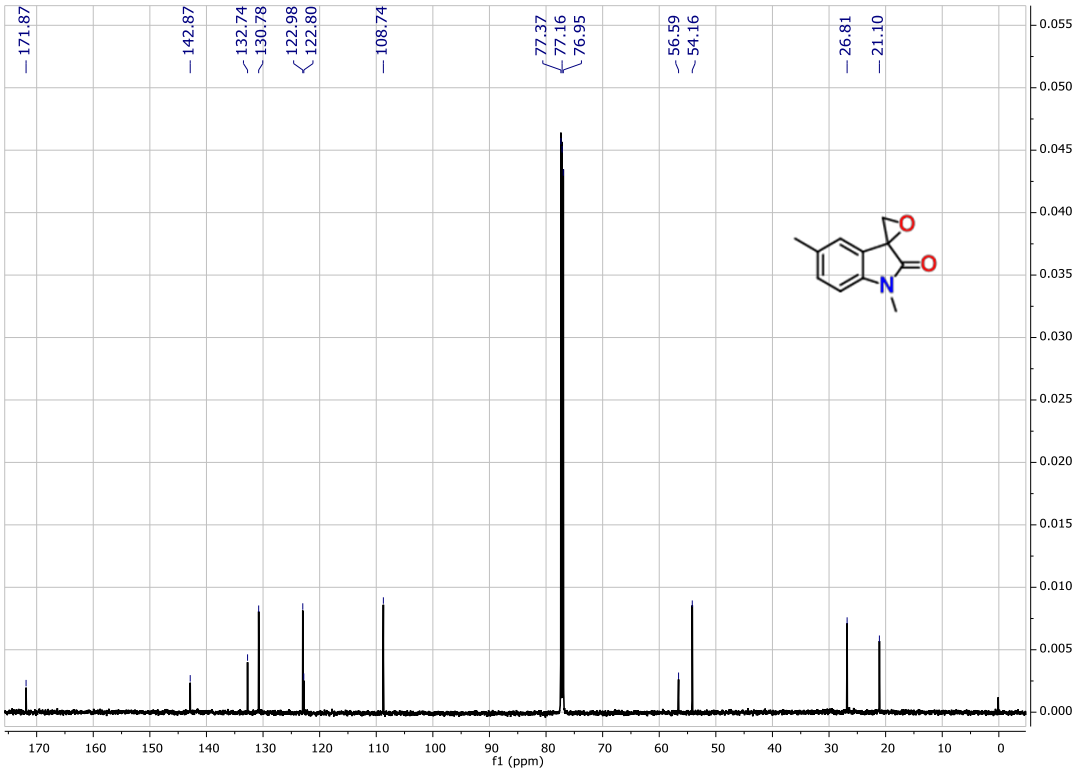

Figure S27. ^{13}C-NMR of the isolated 1,5-dimethylspiro[indoline-3,2'-oxiran]-2-one (S7).

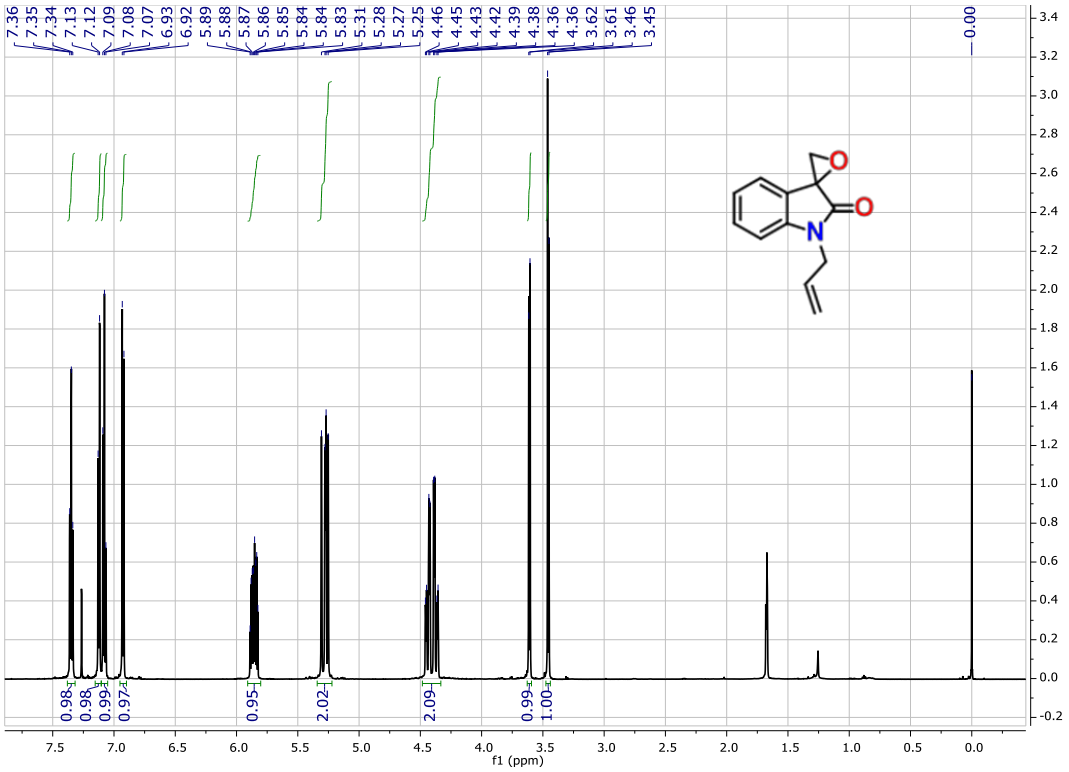

Figure S28. ^{1}H-NMR of the isolated 1-allylspiro[indoline-3,2'-oxiran]-2-one (S8).

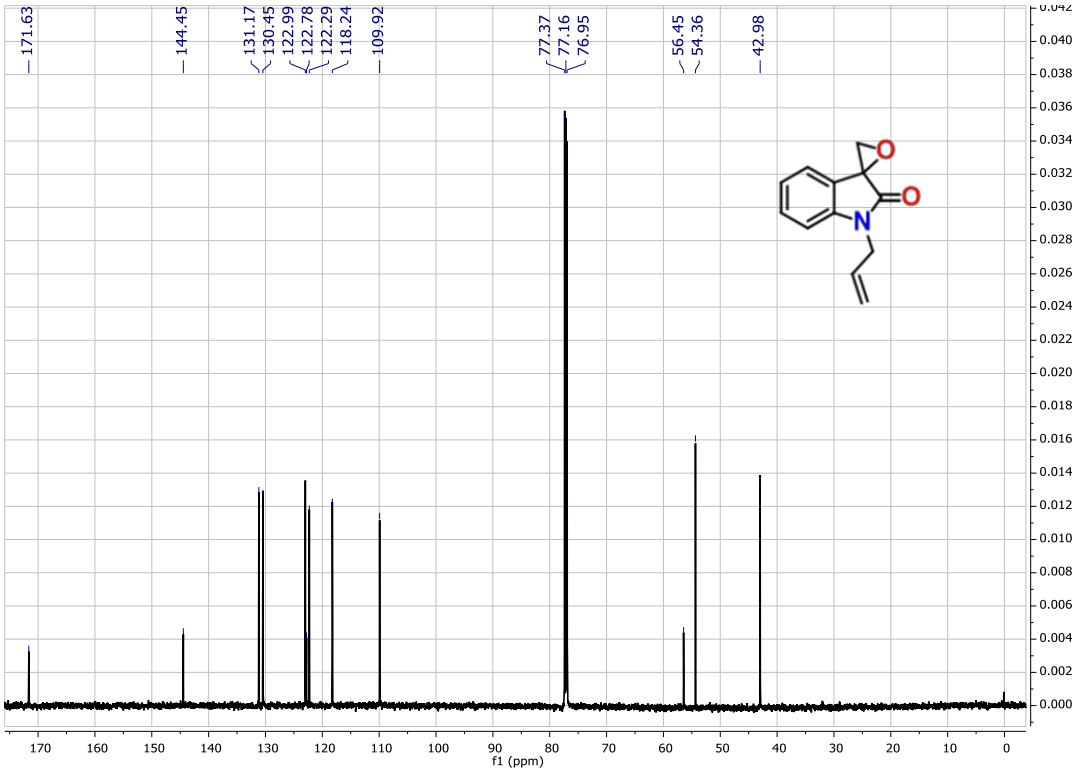

Figure S29. ^{1}H-NMR of the isolated 1-allylspiro[indoline-3,2'-oxiran]-2-one (S8).

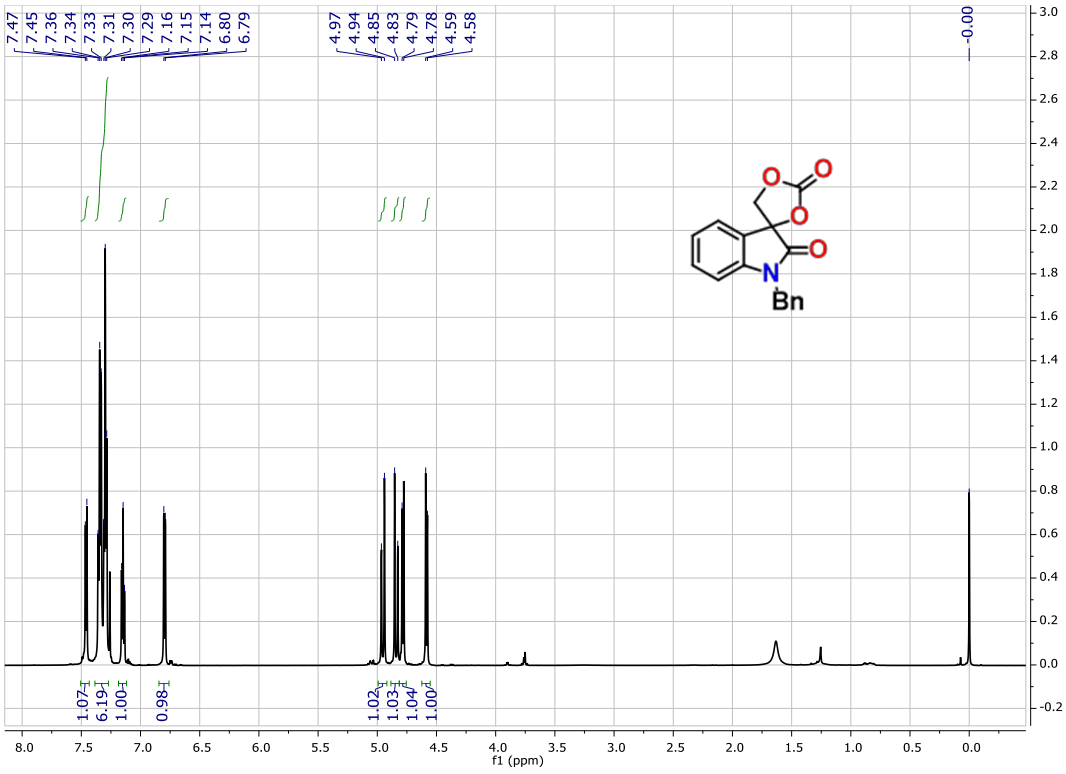

Figure S30. ^{13}C-NMR of the isolated 1-benzylspiro[indoline-3,4'-[1,3]dioxolane]-2,2'-dione (P1).

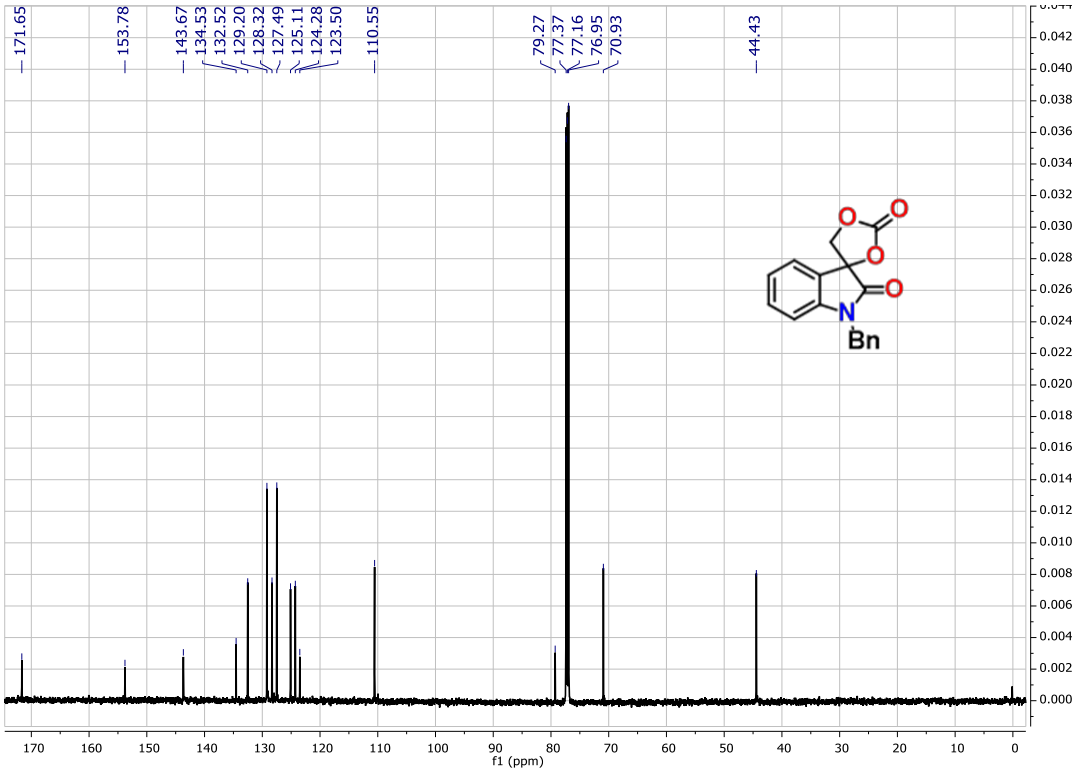

Figure S31. ^{1}H-NMR of the isolated 1-benzylspiro[indoline-3,4'-[1,3]dioxolane]-2,2'-dione (P1).

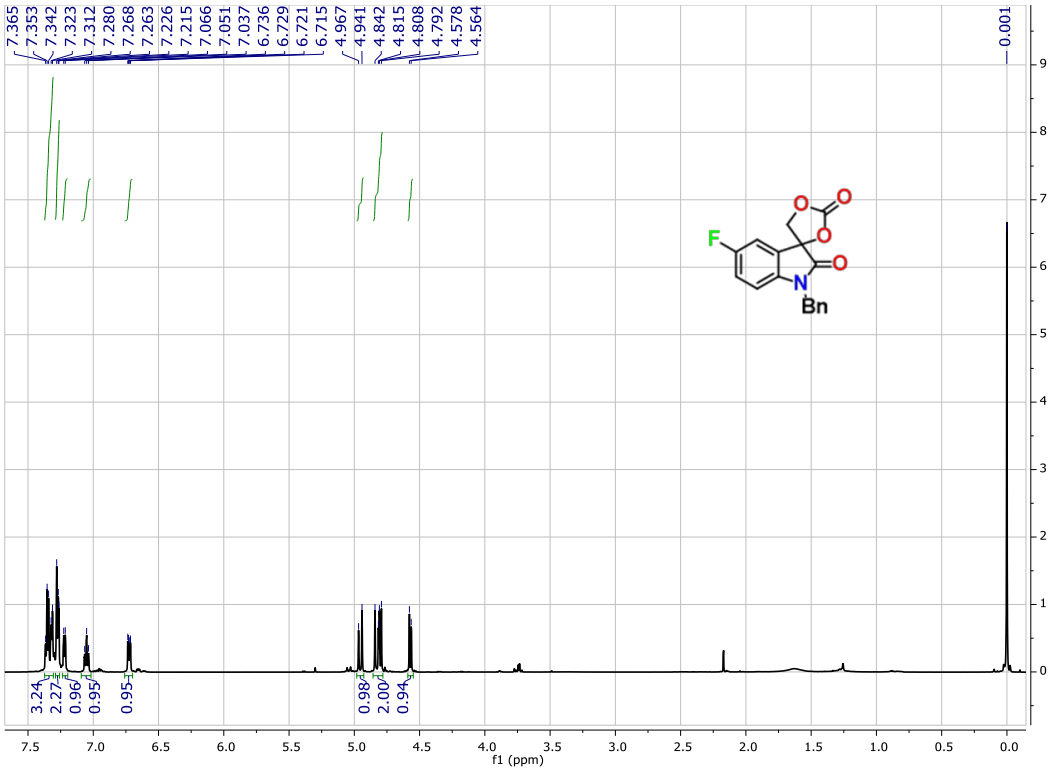

Figure S32. ^{13}C-NMR of the isolated 1-benzyl-5-fluorospiro[indoline-3,4'-[1,3]dioxolane]-2,2'-dione (P2).

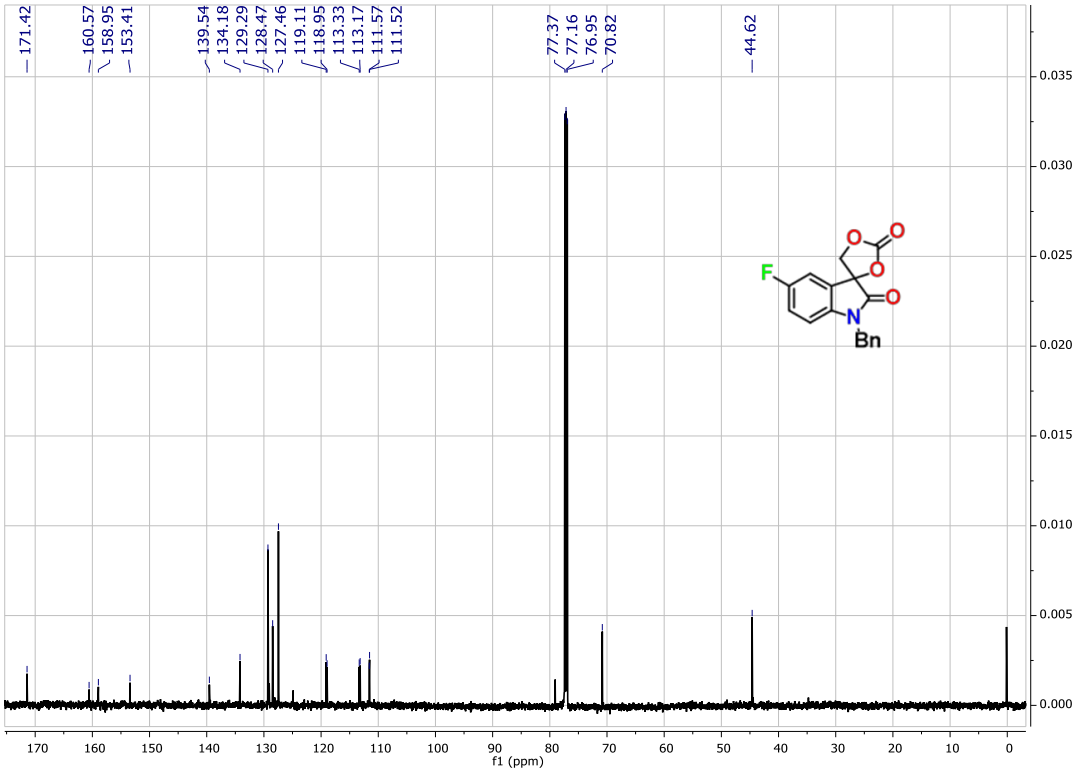

Figure S33. ^{1}H-NMR of the isolated 1-benzyl-5-fluorospiro[indoline-3,4'-[1,3]dioxolane]-2,2'-dione (P2).

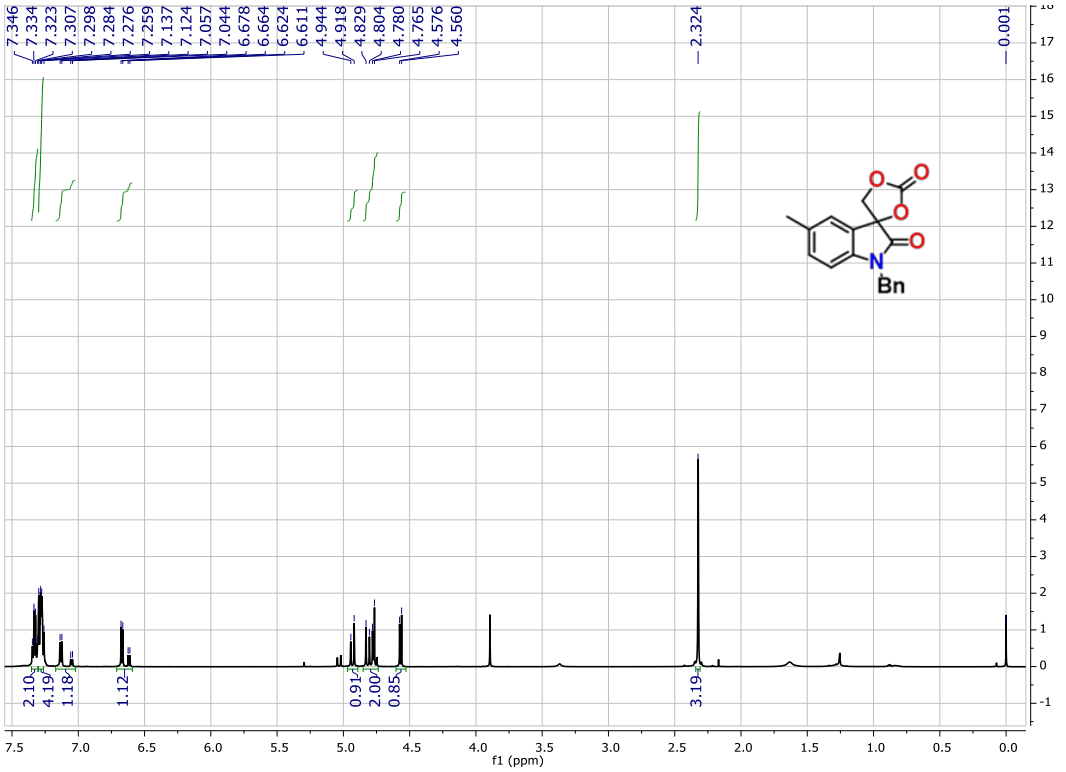

Figure S34. ^{13}C-NMR of the isolated 1-benzyl-5-methylspiro[indoline-3,4'-[1,3]dioxolane]-2,2'-dione (P3).

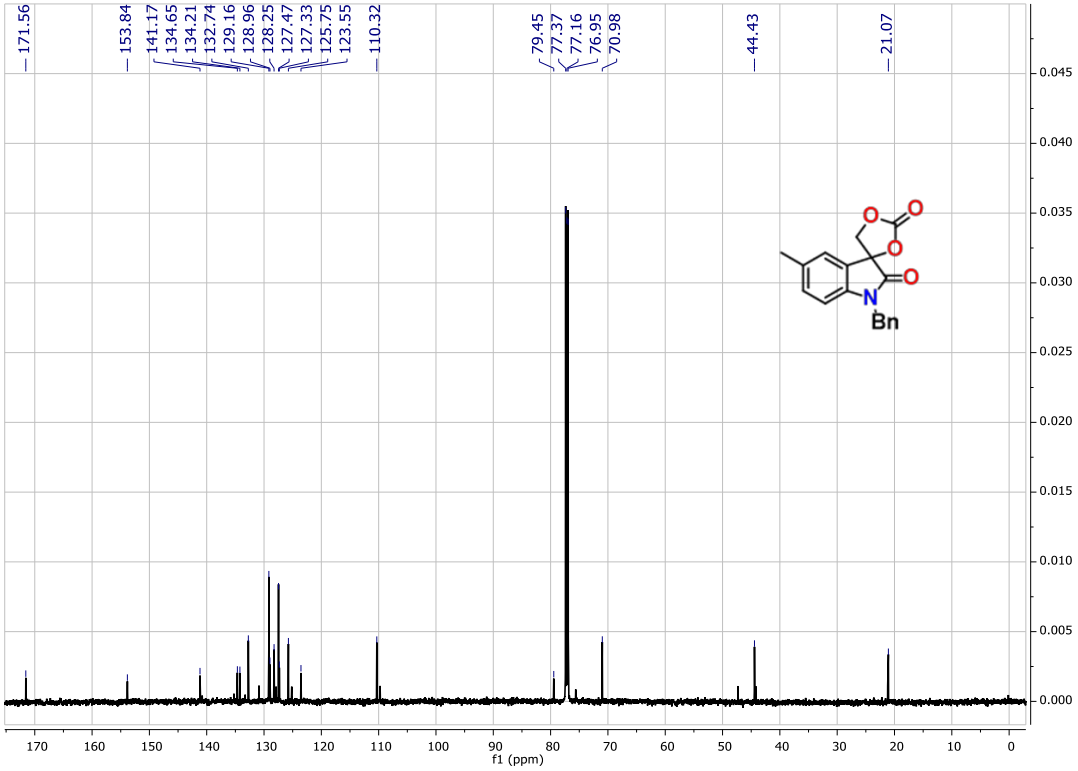

Figure S35. ^{13}C-NMR of the isolated 1-benzyl-5-methylspiro[indoline-3,4'-[1,3]dioxolane]-2,2'-dione (P3).

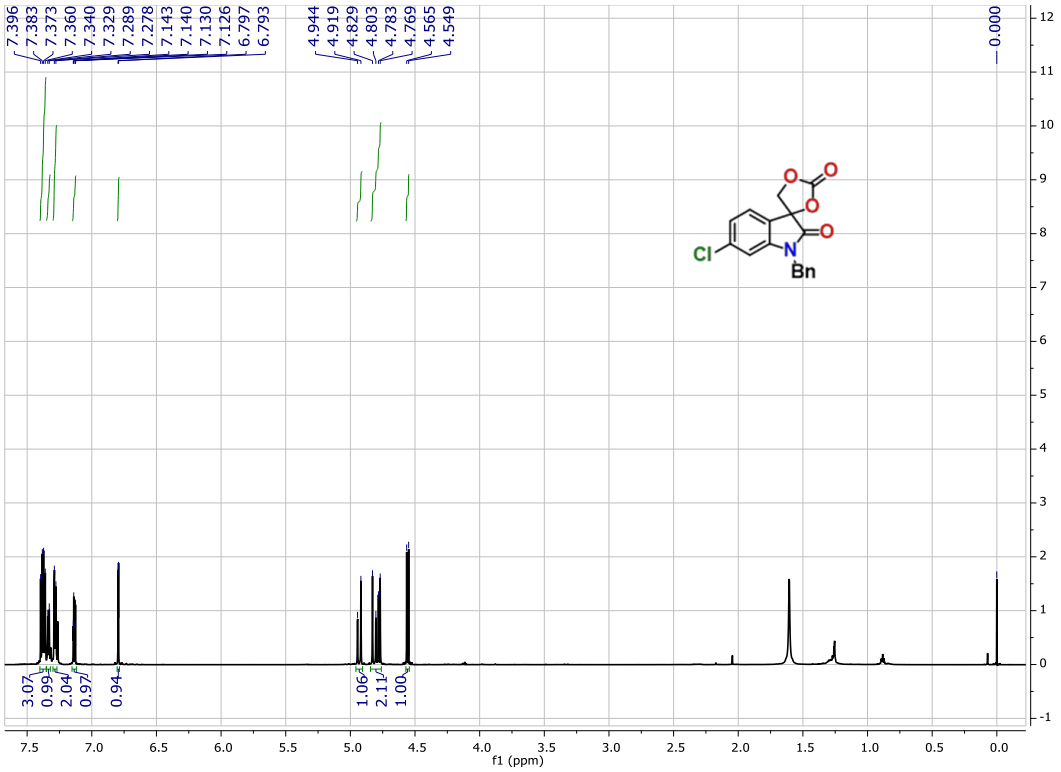

Figure S36. [1]H-NMR of the isolated 1-benzyl-6-chlorospiro[indoline-3,4'-[1,3]dioxolane]-2,2'-dione (P4).

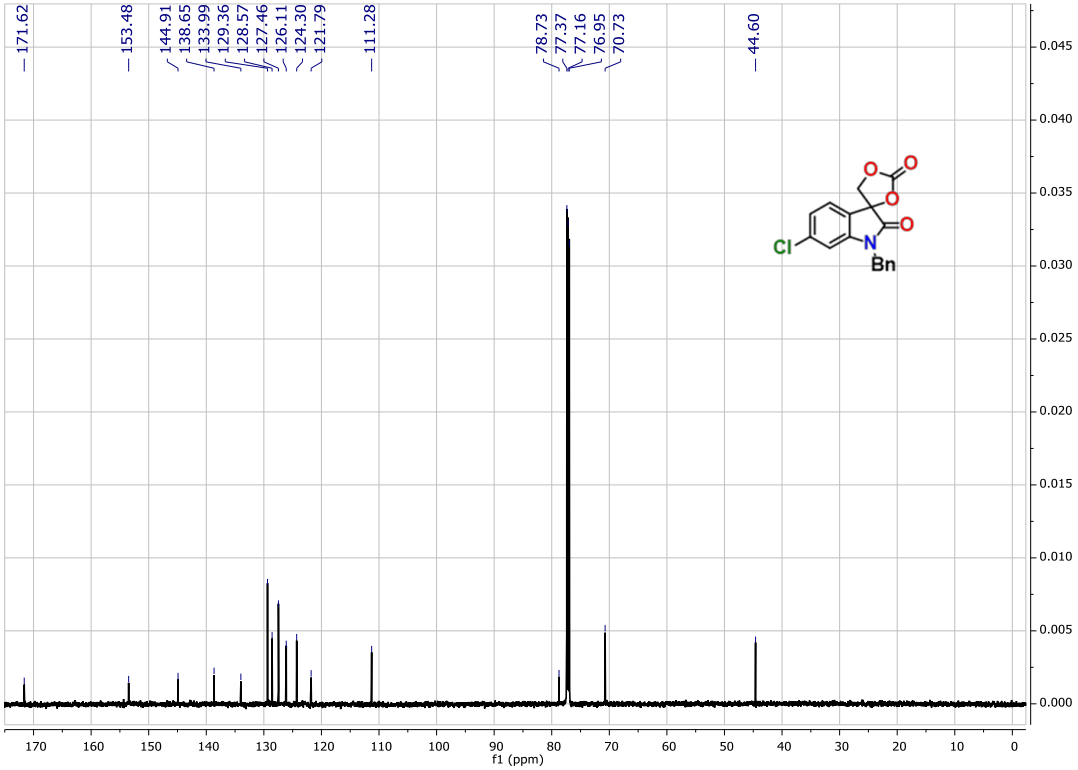

Figure S37. [13]C-NMR of the isolated 1-benzyl-6-chlorospiro[indoline-3,4'-[1,3]dioxolane]-2,2'-dione (P4).

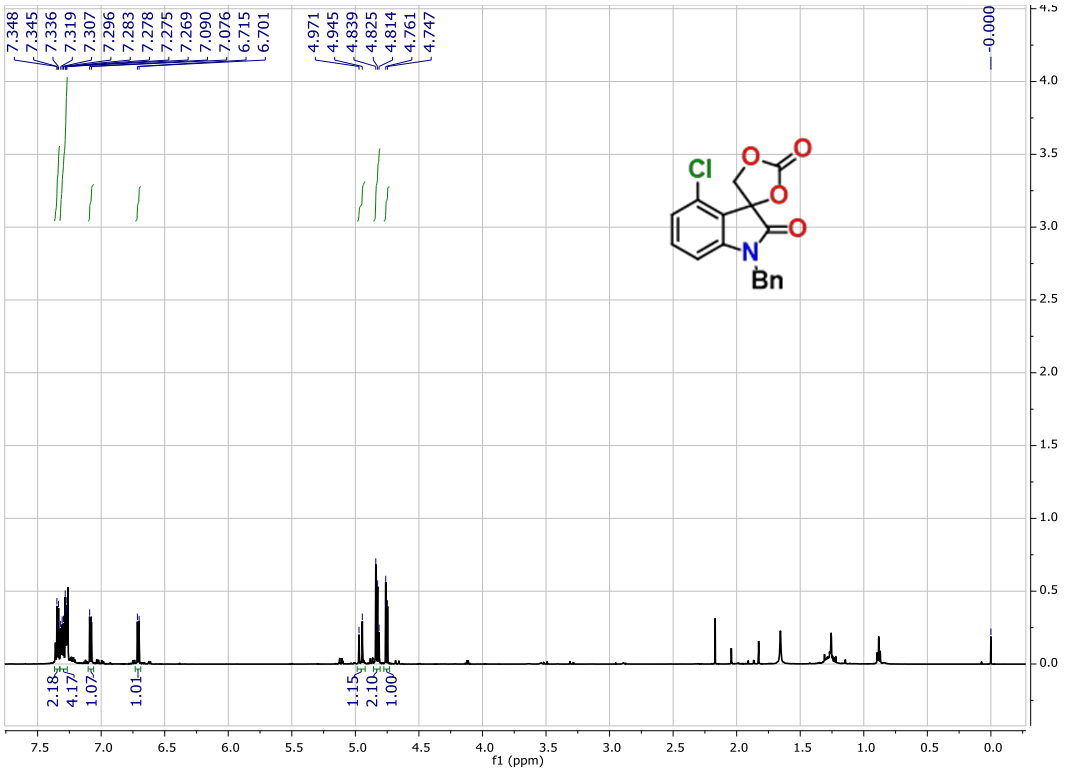

Figure S38. [1]H-NMR of the isolated 1-benzyl-4-chlorospiro[indoline-3,4'-[1,3]dioxolane]-2,2'-dione (P5).

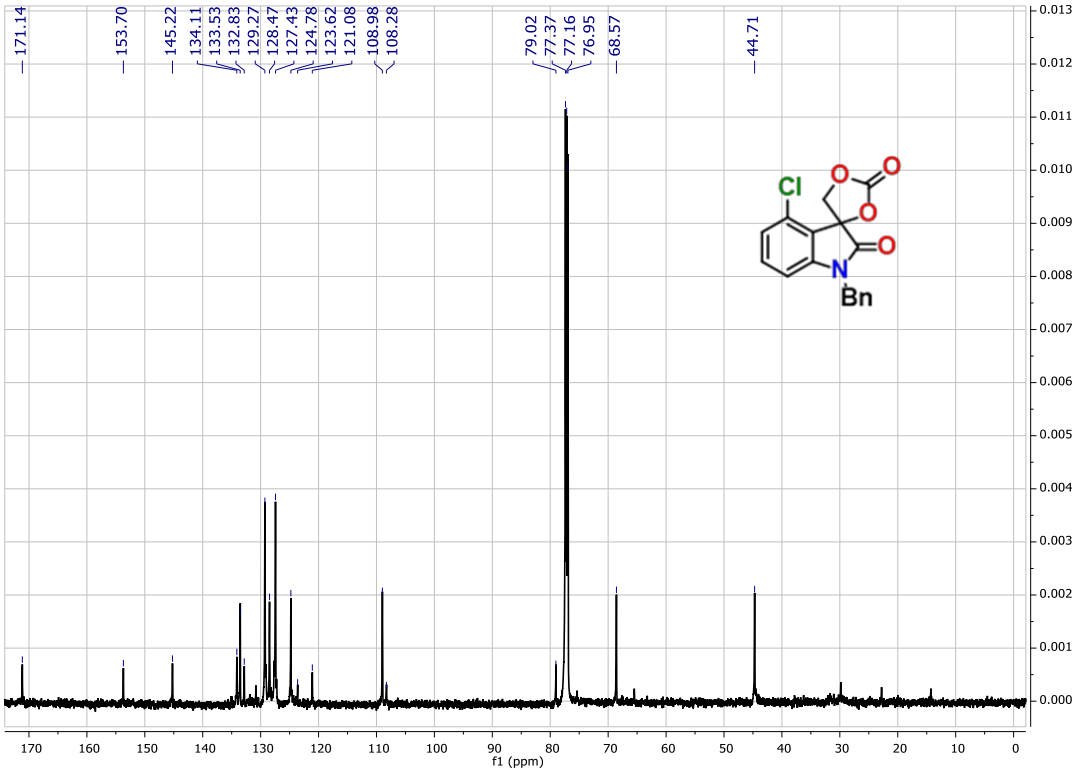

Figure S39. [13]C-NMR of the isolated 1-benzyl-4-chlorospiro[indoline-3,4'-[1,3]dioxolane]-2,2'-dione (P5).

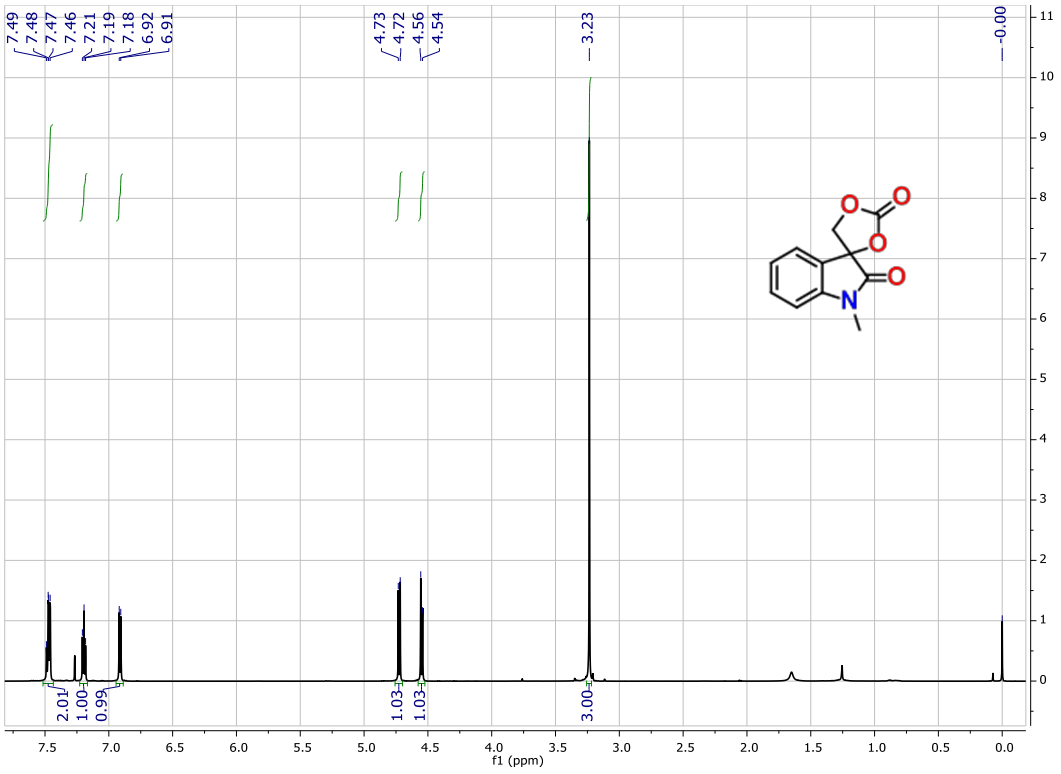

Figure S40. ^{1}H-NMR of the isolated 1-methylspiro[indoline-3,4'-[1,3]dioxolane]-2,2'-dione (P6).

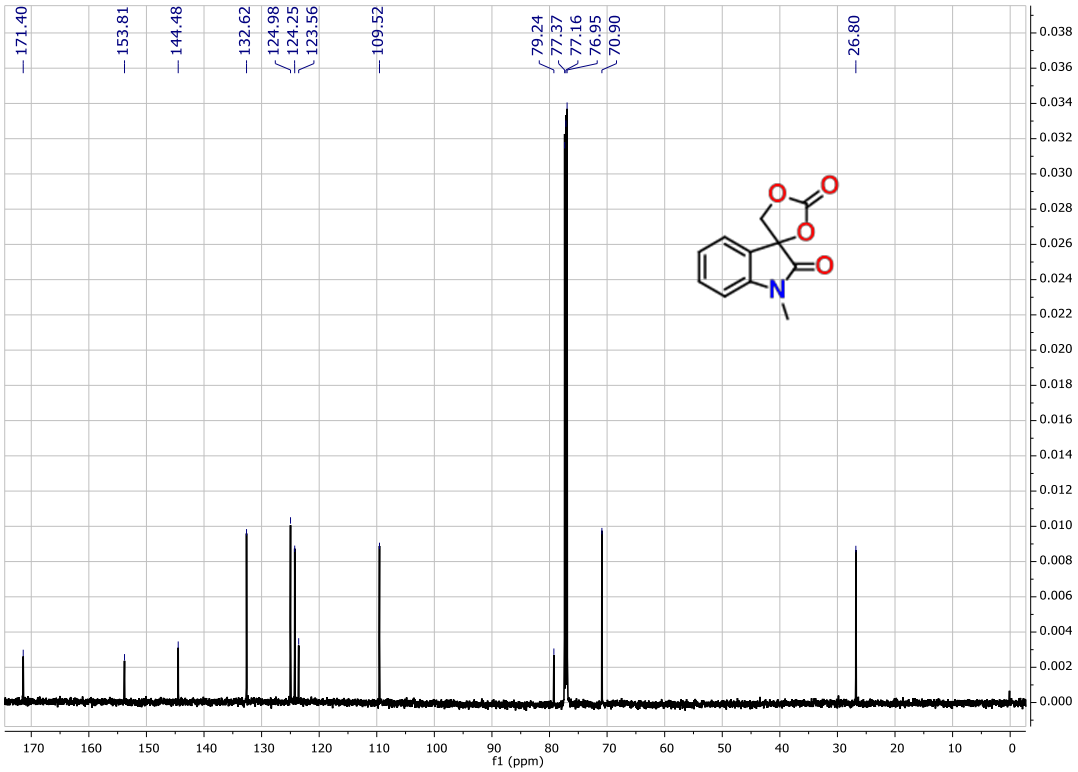

Figure S41. ^{13}C-NMR of the isolated 1-methylspiro[indoline-3,4'-[1,3]dioxolane]-2,2'-dione (P6).

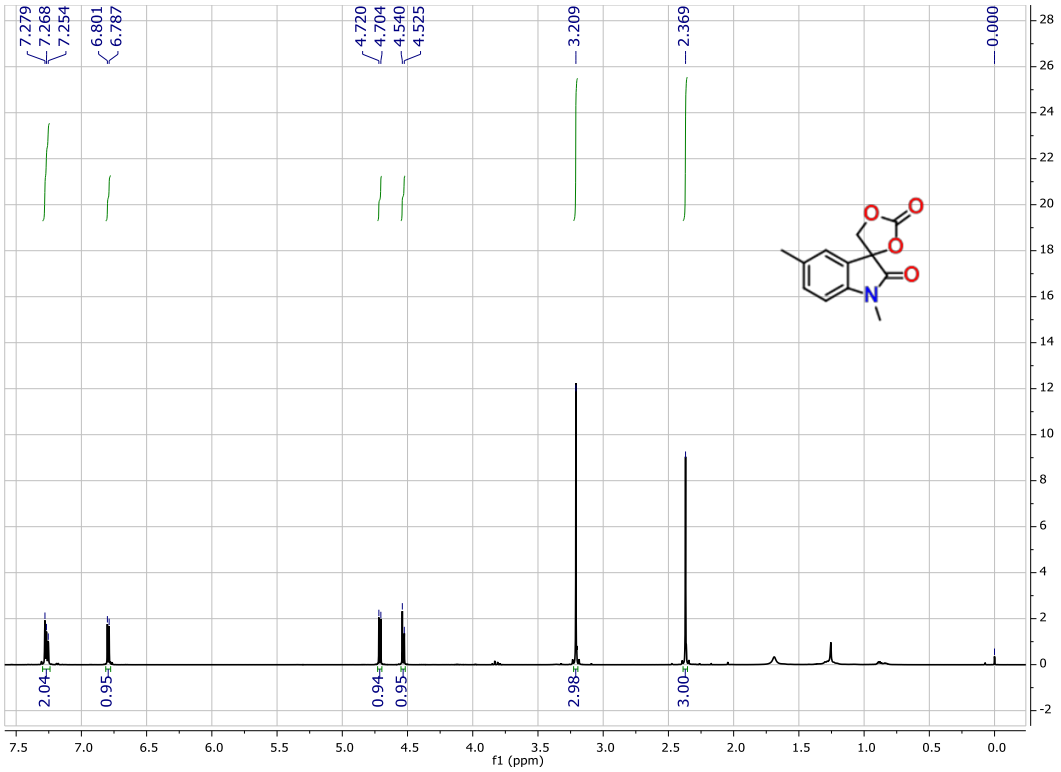

Figure S42. [1]H-NMR of the isolated 1,5-dimethylspiro[indoline-3,4'-[1,3]dioxolane]-2,2'-dione (P7).

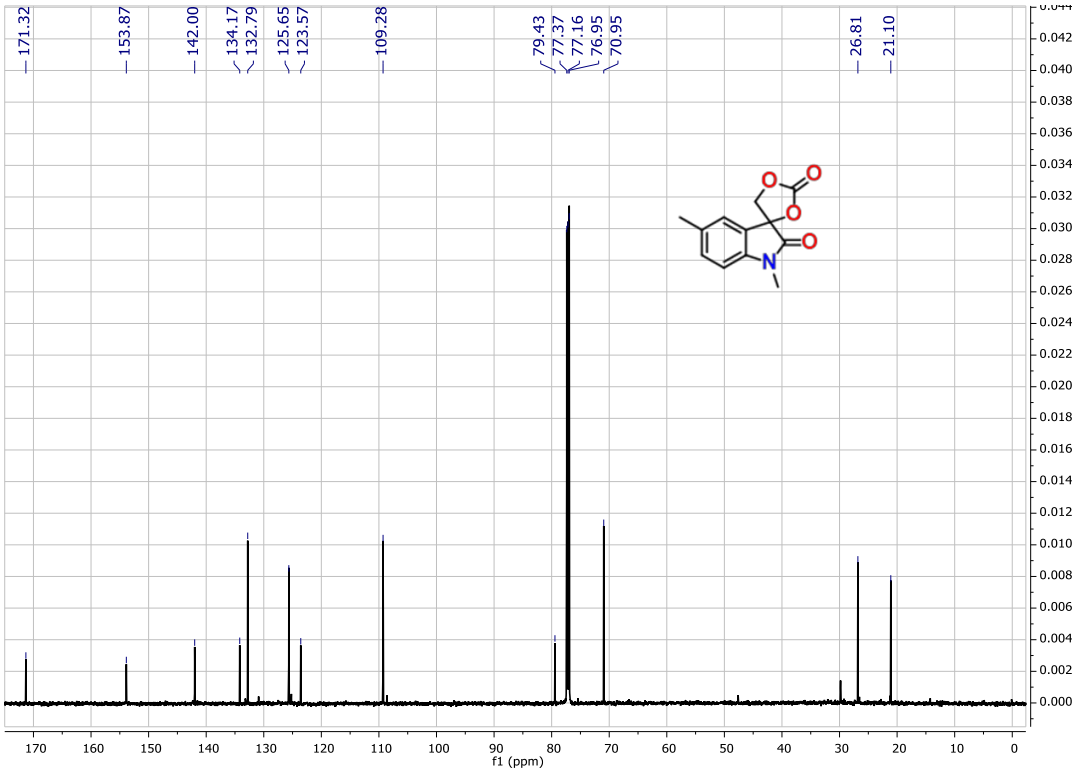

Figure S43. [13]C-NMR of the isolated 1,5-dimethylspiro[indoline-3,4'-[1,3]dioxolane]-2,2'-dione (P7).

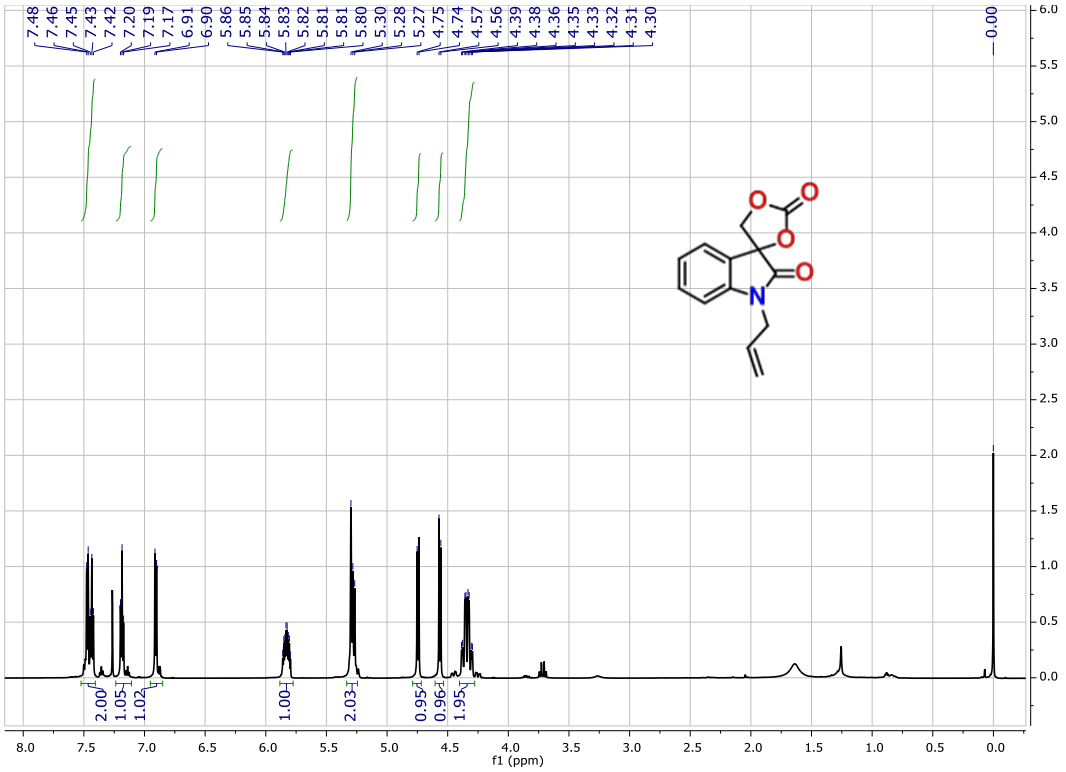

Figure S44. ^{1}H-NMR of the isolated 1-allylspiro[indoline-3,4'-[1,3]dioxolane]-2,2'-dione (P8).

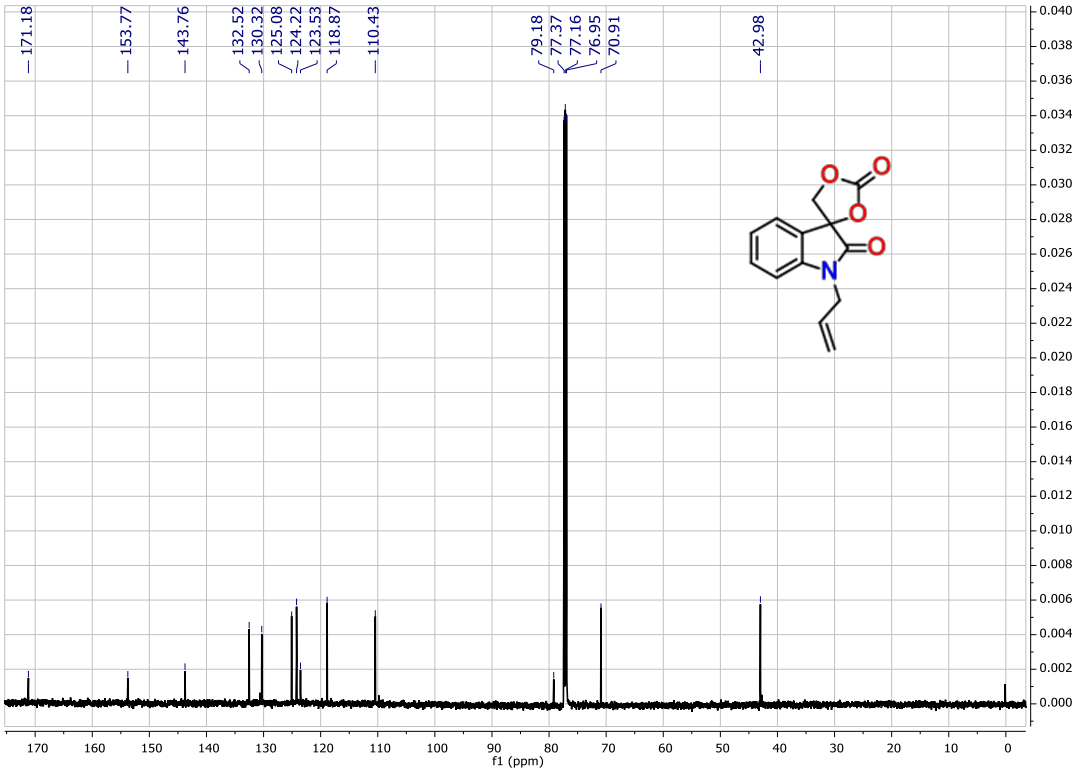

Figure S45. ^{13}C-NMR of the isolated 1-allylspiro[indoline-3,4'-[1,3]dioxolane]-2,2'-dione (P8).

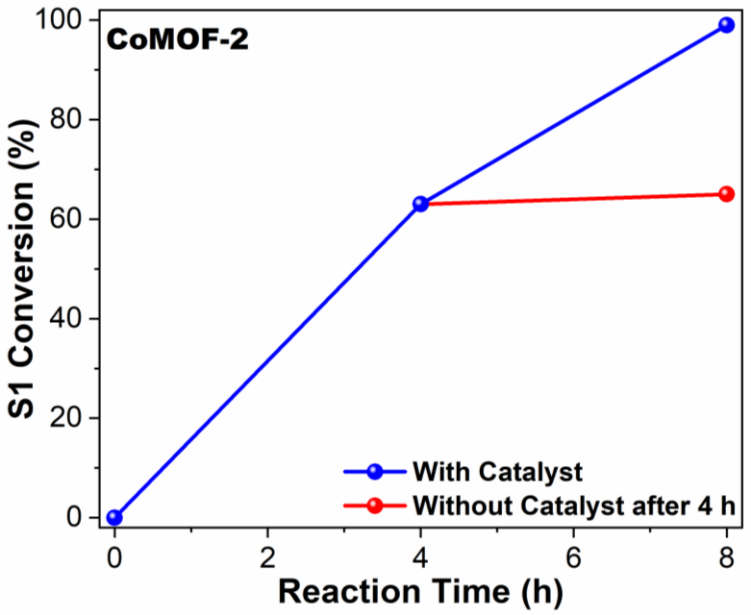

Figure S46. Hot filtration test for cycloaddition reactions catalysed by **CoMOF-2** for metal leaching. [Hot filtration was done at half reaction time].

Table S6. Selected bond length and bond angle for **CoMOF-2**:

CoMOF-2			
Co(1)-O(2)#1	2.007(2)	Co(1)-N(1)	2.158(3)
Co(1)-O(1)	2.014(2)	Co(1)-N(4)#3	2.172(3)
Co(1)-O(4)#2	2.138(2)	Co(1)-O(3)#2	2.271(3)
O(2)#1-Co(1)-O(1)	121.86(11)	N(1)-Co(1)-O(3)#2	92.21(10)
O(2)#1-Co(1)-O(4)#2	148.25(11)	N(4)#3-Co(1)-O(3)#2	89.80(10)
O(1)-Co(1)-O(4)#2	89.69(11)	C(1)-O(1)-Co(1)	150.3(2)
O(2)#1-Co(1)-N(1)	87.32(10)	C(1)-O(2)-Co(1)#1	137.0(2)
O(1)-Co(1)-N(1)	89.45(10)	C(8)-O(3)-Co(1)#4	87.9(2)
O(4)#2-Co(1)-N(1)	89.73(11)	C(8)-O(4)-Co(1)#4	93.9(2)
O(2)#1-Co(1)-N(4)#3	90.80(10)	C(13)-N(1)-Co(1)	123.3(2)
O(1)-Co(1)-N(4)#3	89.82(10)	C(9)-N(1)-Co(1)	120.6(2)
O(4)#2-Co(1)-N(4)#3	92.93(11)	C(18)-N(4)-Co(1)#5	121.9(2)
N(1)-Co(1)-N(4)#3	177.24(10)	C(19)-N(4)-Co(1)#5	121.0(2)
O(2)#1-Co(1)-O(3)#2	89.80(10)	O(1)-C(1)-O(2)	125.1(3)
O(1)-Co(1)-O(3)#2	148.35(10)	O(3)-C(8)-O(4)	119.5(3)
O(4)#2-Co(1)-O(3)#2	58.72(10)	-----	----
Symmetry transformation: #1 5/2-x,3/2-y,-z #2 5/2-x,1/2+y,1/2-z #3 1+x,+y,+z #4 5/2-x,-1/2+y,1/2-z #5 -1+x,+y,+z			

Table S7. Details of hydrogen bonding interactions observed in the structure of **CoMOF-2**:

D-H···A	d(H···A) (Å)	d(D···A) (Å)	∠D-H···A (°)
CoMOF-2			
N(3)-H(3C)···O(7)[1]	2.05	2.910(5)	164
O(6)-H(6C)···O(5)[2]	2.02(3)	2.907(5)	157(3)
O(6)-H(6D)···O(4)[3]	1.93(3)	2.839(5)	157(3)
O(7)-H(7D)···O(3)[4]	1.85(3)	2.790(5)	166(3)
C(20)-H(20)···O(7)[1]	2.42	3.340(5)	164
Symmetry code: 1. 3/2-x,3/2-y,-z 2. x,y,z 3. 2-x,y,1/2-z 4. -1/2+x,1/2+y,z			

References:

S1. *SAINT+, 6.02 ed*, Bruker AXS, Madison, WI, 1999.

S2. *XPREP, 5.1 ed*, Siemens Industrial Automation Inc., Madison, WI, 1995.

S3. Sheldrick, G. M. *SHELXTL Reference Manual: Version 5.1*; Bruker AXS, Madison, WI, 1997.

S4. Sheldrick, G. M. Crystal structure refinement with SHELXL. *Acta Cryst. C* **2015**, *71*, 3-8.

S5. Spek, A. L. Single-crystal structure validation with the program PLATON. *J. Appl. Crystallogr.* **2003**, *36*, 7-13.

S6. Vandersluis, P.; Spek, A. L. BYPASS: an effective method for the refinement of crystal structures containing disordered solvent regions. *Acta Crystallogr., Sect. A* **1990**, *46*, 194-201.

S7. Tak, R. K.; Patel, P.; Subramanian, S.; Kureshy, R. I.; Khan, N. H. Cycloaddition Reaction of Spiro-Epoxy Oxindole with CO_2 at Atmospheric Pressure Using Deep Eutectic Solvent. *ACS Sustainable Chem. Eng.* **2018**, *6*, 11200-11205.

S8. VandeVondele, J.; Krack, M.; Mohamed, F.; Parrinello, M.; Chassaing, T.; Hutter, J. Quickstep: Fast and accurate density functional calculations using a mixed Gaussian and plane waves approach. *Comput. Phys. Commun.* **2005**, *167*, 103-128.

S9. VandeVondele, J.; Hutter, J. An efficient orbital transformation method for electronic structure calculations. *J. Chem. Phys.* **2003**, *118*, 4365-4369.

S10. Lippert, G.; Hutter, J.; Parrinello, M. The Gaussian and augmented-plane-wave density functional method for ab initio molecular dynamics simulations. *Theor. Chem. Acc.* **1999**, *103*, 124-140.

S11. Lippert, B. G.; Hutter, J.; Parrinello, M. A hybrid Gaussian and plane wave density functional scheme. *Mol. Phys.* **1997**, *92*, 477-487.

S12. Perdew, J. P.; Wang, Y. Accurate and simple density functional for the electronic exchange energy: Generalized gradient approximation. *Phys. Rev. B* **1986**, *33*, 8800-8802.

S13. VandeVondele, J.; Hutter, J. Gaussian basis sets for accurate calculations on molecular systems in gas and condensed phases. *J. Chem. Phys.* **2007**, *127*, 114105.

S14. Goedecker, S.; Teter, M.; Hutter, J. Separable dual-space Gaussian pseudopotentials. *Phys. Rev. B.* **1996**, *54*, 1703-1710.

S15. Grimme, S.; Antony, J.; Ehrlich, S.; Krieng, H.; A consistent and accurate ab initio parametrization of density functional dispersion correction (DFT-D) for the 94 elements H-Pu. *J. Chem. Phys.* **2010**, *132*, 154104.

S16. Campana, C.; Mussard, B.; Woo, T. K. Electrostatic Potential Derived Atomic Charges for Periodic Systems Using a Modified Error Functional. *J. Chem. Theory Comput.* **2009**, *5*, 2866-2878.

S17. Golze, D.; Hutter, J.; Iannuzzi, M. Wetting of water on hexagonal boron nitride@Rh(111): a QM/MM model based on atomic charges derived for nano-structured substrates. *Phys. Chem. Chem. Phys.* **2015**, *17*, 14307-14316.

S18. Rappé, A. K.; Casewit, C. J.; Colwell, K. S.; Goddard III, W. A.; Skiff, W. M. UFF, a full periodic table force field for molecular mechanics and molecular dynamics simulations. *J. Am. Chem. Soc.* **1992**, *114*, 10024-10035.

S19. Harris, J. G.; Yung, K. H. Carbon Dioxide's Liquid-Vapor Coexistence Curve and Critical Properties as Predicted by a Simple Molecular Model. *Phys. Chem.* **1995**, *99*, 12021-12024.

S20. Dubbeldam, D.; Calero, S.; Ellis, D. E.; Snurr, R. Q. RASPA: molecular simulation software for adsorption and diffusion in flexible nanoporous materials. *Mol. Simulat.* **2016,** *42*, 81-101.

S21. Peng, D. -Y.; Robinson, D. B. A New Two-Constant Equation of State. *Ind. Eng. Chem. Fundam.* **1976**, *15*, 59-64.

S22. Vlugt, T. J. H.; García-Pérez, E.; Dubbeldam, D.; Ban, S.; Calero, S. Computing the Heat of Adsorption Using Molecular Simulations: The Effect of Strong Coulombic Interactions. *J. Chem. Theory Comput.* **2008**, *4*, 1107-1118.

S23. Zhao, Y.; Truhlar, D. G. The M06 suite of density functionals for main group thermochemistry, thermochemical kinetics, noncovalent interactions, excited states, and transition elements: two new functionals and systematic testing of four M06-class functionals and 12 other functionals. *Theor. Chem. Acc.* **2008**, *120*, 215-241.

S24. Frisch, M. J.; Trucks, G. W.; Schlegel, H. B.; Scuseria, G. E.; Robb, M. A.; Cheeseman, J. R.; Scalmani, G.; Barone, V.; Petersson, G. A.; Nakatsuji, H.; Li, X.; Caricato, M.; Marenich, A. V.; Bloino, J.; Janesko, B. G.; Gomperts, R.; Mennucci, B.; Hratchian, H. P.; Ortiz, J. V.; Izmaylov, A. F.; Sonnenberg, J. L.; Williams-Young, D.; Ding, F.; Lipparini, F.; Egidi, F.; Goings, J.; Peng, B.; Petrone, A.; Henderson, T.; Ranasinghe, D.; Zakrzewski, V. G.; Gao, J.; Rega, N.; Zheng, G.; Liang, W.; Hada, M.; Ehara, M.; Toyota, K.; Fukuda, R.; Hasegawa, J.; Ishida, M.; Nakajima, T.; Honda, Y.; Kitao, O.; Nakai, H.; Vreven, T.; Throssell, K.; Montgomery, J. A., Jr.; Peralta, J. E.; Ogliaro, F.; Bearpark, M. J.; Heyd, J. J.; Brothers, E. N.; Kudin, K. N.; Staroverov, V. N.; Keith, T. A.; Kobayashi, R.; Normand, J.; Raghavachari, K.; Rendell, A. P.; Burant, J. C.; Iyengar, S. S.; Tomasi, J.; Cossi, M.; Millam, J. M.; Klene, M.; Adamo, C.; Cammi, R.; Ochterski, J. W.; Martin, R. L.; Morokuma, K.; Farkas, O.; Foresman, J. B.; Fox, D. J. *Gaussian 16, Revision B.01,* Gaussian, Inc., Wallingford CT, **2016**.

S25. Chouhan, M.; Senwar, K. R.; Sharma, R.; Grover. V.; Nair, V. A. Regiospecific epoxide opening: a facile approach for the synthesis of 3-hydroxy-3-aminomethylindolin-2-one derivatives. *Green Chem.* **2011**, *13*, 2553-2560.

S26. Tak, R. K.; Gupta, N.; Kumar, M.; Kureshy, R. I.; Khan, N. H.; Suresh, E. Regioselective Alcoholysis and Hydrochlorination Reactions of Spiro-Epoxy Oxindoles at the Spiro-Centre: Synthesis of 3,3-Disubstituted Oxindoles and Application for Anticancer Agents. *Eur. J. Org. Chem.* **2018**, 5678-5687.